Spectroscopy of two-field Inflation

Welling, Y.M.

Introduction

Cosmology is a fascinating field of research. The advance of theory and observations in the last centuries has enabled us to reformulate philosophical musings such as "Where do we come from?" as quantitatively testable scientific questions. It is impressive that we have been able to learn about the universe far in the past. This resulted in the Hot Big Bang model: an excellent description of the universe from the moment it was merely a few minutes old. Moreover, cosmological inflation has provided us with a very compelling model of the primordial universe. It predicts the creation of seeds of structure formation from quantum perturbations at that time. Therefore, we might still find an imprint of the primordial universe in the sky. This allows us to look back to perhaps[1] the first $10^{-30}s$, a mind-blowing thought! At that time the universe was extremely dense and tiny and thus dominated by ultra high energy particle physics. Therefore, inflation connects observations on cosmological scales to particle physics not accessible at earth-based particle accelerators. In other words, inflation provides the ultimate playground for a theoretical physicist.

In the main part of this thesis we aim to improve our understanding of the signatures of new physics at the time of inflation. Additionally, in the second part we perform a statistical analysis to understand whether we can extract some of the traces thereof from the 3D map of galaxies in the near future.

Throughout this thesis we work in Planck units $\hbar = c = k_B = 1$ and the reduced Planck mass is given by $M_p = (8\pi G)^{-1/2}$.

[1] Please take the time-scale of inflation with a grain of salt, it is a model dependent number. It could as well be a factor of a million off, but nevertheless it is still extremely small.

1.1 A brief history of modern cosmology

Most of modern research in cosmology is based on the Standard Model of Cosmology. For my generation of cosmologists the so-called ΛCDM model is a natural starting point, but from a historical point of view it must have been quite some journey to get here. The road was bumpy and the passage required several radically new ideas. Due to the efforts of many great scientists, ΛCDM was established within a century. In this section I aim to give an idea of the historical development of ΛCDM. This section is mainly based on [1–6].

1.1.1 The hot Big Bang model

An expanding universe

Einstein's General Relativity (GR) [7] marked the beginning of cosmology as a predictive science. The dynamical and geometrical properties of the universe are related to its constituents by the Einstein equations. One key property follows from the premise that there are no privileged positions or directions in the universe. More precisely, the *Cosmological Principle* states that the universe is statistically homogeneous and isotropic at large scales.

Einstein believed in a static universe, and in 1917 he introduced [8] the static cosmological model as a homogeneous and isotropic solution to GR. For that purpose he famously introduced the *cosmological constant*. It turned out that this solution is unstable [9]. Around the same time De Sitter [10] published another 'static' cosmological model, which in fact described an exponentially expanding universe (but this was only realized later by Lemaître.) It corresponds to a universe with no matter, but only a cosmological constant. He calculated that this would result in a redshift of distant sources and he realized that this could explain the observation of Slipher [11].

In the following decades substantial observational and theoretical progress was made. On the theory side, the most general cosmological solution of a homogeneous and isotropic universe was established: today we call it the Friedmann-Lemaître-Robertson-Walker (FLRW) metric [12–16]

$$ds^2 = -dt^2 + a(t)^2 \left(\frac{dr^2}{1-\kappa r^2} + r^2 \left(d\theta^2 + \sin^2\theta \, d\phi^2 \right) \right) \tag{1.1}$$

Here the constant $\kappa \in \{-1, 0, 1\}$ denotes whether the curvature of the spatial slices is negatively curved, flat or positively curved, respectively. The *scale factor* $a(t)$ probes the *physical* distance between two points on the *comoving* spatial slice at the time t. It is a measure of the relative size of the universe

compared to today, i.e. $a(t_0) = 1$. The expansion rate of the universe is measured by the *Hubble parameter* $H(t) \equiv \frac{\dot{a}(t)}{a(t)}$. The stress-energy tensor corresponding to the FLRW spacetime is that of a homogeneous and isotropic fluid with pressure p and energy density ρ. The evolution of the universe, as parameterized by the Hubble parameter, can therefore be related to its matter content by the Friedmann equations

$$H^2 \equiv \frac{\dot{a}^2}{a^2} = \frac{\rho}{3M_p^2} - \frac{\kappa^2}{a^2}, \tag{1.2a}$$

$$\dot{\rho} + 3H\,(\rho + p) = 0\ . \tag{1.2b}$$

Only when $a(t)$ is constant, or $H = 0$, this resembles the static solution of Einstein. A constant Hubble parameter H, and therefore $a \sim e^{Ht}$, corresponds to the De Sitter solution.

Lemaître [14] realized that a non-static universe, i.e. $H(t) \neq 0$, leads to *cosmological redshift* of photons. Photons moving freely in an expanding spacetime lose their energy like $E \sim a^{-1}$. In other words their wavelength stretches, and spectra emitted by distant objects redshift. He understood that the 'apparent velocity' of galaxies as measured by Slipher [11] and Hubble [17] was in fact mainly caused by the expansion of spacetime[2]. He also provided the linear velocity-distance relation

$$v = Hd\ . \tag{1.3}$$

This is now called *Hubble's law*[3] , after [20].

Big Bang nucleosynthesis

The observation that the universe is expanding led Lemaître [21] to propose the tantalizing idea that the universe must have been much smaller and denser in the past. His idea was first met with contempt by his peers; Fred Hoyle even coined the term 'Big Bang' to make fun of Lemaître. However, in 1984 his idea was put on firmer ground when Gamow and collaborators [22] used his idea to predict the formation of light elements during the first three minutes. They

[2] An earlier interpretation came from his mentor Eddington [18], based on Slipher's measurements of 36 redshifted spiral nebulae in the 1910s. He concluded that De Sitter's solution provided an explanation: "there is the general displacement of spectral lines to the red in distant objects due to the slowing down of atomic vibration which would be erroneously interpreted as a motion of recession." Moreover, Lemaître reanalysed the result of De Sitter in [19] for which he found the linear velocity-distance relation.

[3] Apparently, in the English translation of Lemaître's article, the relevant lines about velocity-distance relation were modified [1].

had the crucial insight that the nuclear reactions could take place because the early universe was radiation dominated and very *hot*. This was the birth of the *Hot Big Bang* model, in which *Big Bang Nucleosynthesis* (BBN) plays a key role. However, it took the detection of the Cosmic Microwave Background radiation (see below), before the Hot Big Bang scenario became accepted by the scientific community. Nowadays, the relative abundances of light elements are well-tested and - except for the Lithium abundance - in good agreement with late time observations [23–25].

Cosmic Microwave Background radiation

Soon after, also in 1948, Alpher and Hermann [26] predicted that we should see an afterglow of the Hot Big Bang. At early times, radiation was in thermal equilibrium with matter. Only after 380.000 years, when the universe cooled down to temperatures $T \sim 3000K$ such that neutral hydrogen could be formed (recombination), the number of free electrons dropped enormously. Thomson scattering, coupling photons to free electrons, became inefficient and photons started to freestream (decoupling). These photons have been travelling since then, while being redshifted with the expansion of the universe. Alpher and Hermann predicted that today we are immersed in a bath of thermal photons of temperature $T \sim 5K$. Almost twenty years later Penzias and Wilson [27] discovered a mysterious isotropic antenna noise, which turned out to be the *Cosmic Microwave Background* radiation (CMB). In 1993 the COBE mission confirmed their measurement and showed that it follows a blackbody spectrum [28] with average temperature $T \approx 2.7K$. Moreover, the COBE team found [29] small variations in the temperature of order 10^{-5}, reflecting small density inhomogeneities crucial for structure formation in the late universe. Figure 1.1 shows the most recent map of the CMB temperature variations from the *Planck* collaboration [30]

1.1.2 Dark matter and dark energy

Accepting the Hot Big Bang picture of an expanding universe, the next step was to understand its constituents and its geometry. For that purpose it is useful to define the *critical density* for which the universe is flat ($\kappa = 0$)

$$\rho_c \equiv 3M_p^2 H^2 \ . \tag{1.4}$$

The ratio of the total energy density to the critical density, i.e. the *density parameter* $\Omega \equiv \frac{\rho}{\rho_c}$ is a measure of the geometry of the universe. If $\Omega = 1$ the universe is flat, if $\Omega < 1$ the universe is open ($\kappa = -1$) and if $\Omega > 1$ the universe is closed ($\kappa = 1$).

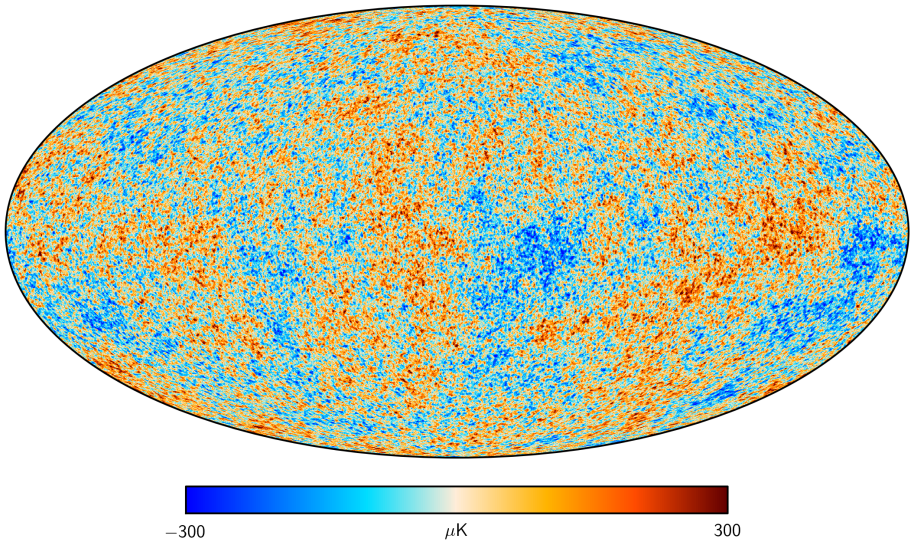

Figuur 1.1: The CMB intensity map as measured by *Planck* [30]. The colours represent small temperature variations of order 10^{-5} with respect to the background $T \sim 2.73K$.

The BBN computations of Gamow and collaborators [22] provided the first theoretical prediction of the amount of baryonic matter in the universe. This was possible, because there is only a short window in time for nucleosynthesis to take place. The abundance of light elements depends on two parameters: the expansion rate of the universe (matter to radiation ratio) and the density of neutrons and protons (*baryonic matter*). The prediction of Gamow et al was consistent with the observed matter density in galaxies and intervening gases, namely a few percent of the critical density. However, this number was a bit puzzling for another reason. Observations of the rotation curves of the outer parts of galaxies, starting with the measurements of Babcock [31] and Oort [32], suggested that the amount of matter in a galaxy should be much higher, about 20-30 percent of the critical density.

Meanwhile, after the establishment of the Hot Big Bang model and with the first all-sky redshift surveys of galaxies, Peebles' picture of hierarchical structure formation by gravitational clustering [33] gained more support. This led astronomers to look for temperature variations in the CMB as a proxy for the amplitude of initial density fluctuations. However, already in the late 70s it was clear that the temperature fluctuations were too small to account for all the observed structures [34]. This led several astronomers to suggest the existence of non-baryonic matter. This idea was not new, because the ear-

lier observations of Kapteyn [35] (reinterpreted by Jeans [36]) and Zwicky [37] indicated the presence of invisible matter, or *dark matter*. Decisive evidence of dark matter came with the high precision observations of the flattening of galaxy rotation curves by Rubin [38]. The only known non-baryonic matter particle was the neutrino, but it was soon realized that its velocity dispersion is too high to support structure formation on galactic scales. Therefore, several *Cold Dark Matter* (CDM) scenarios were proposed [39–43]. The important property of CDM is that it has to move with non-relativistic velocities in the early universe. In addition, the CDM model solved the missing matter problem described above, so it killed two birds with one stone. Therefore, even though CDM is of unknown nature up until today, it became part of our modern cosmological model.

So far so good. A more coherent picture of the contents of the universe started to emerge. It was believed that the universe contains radiation and both visible and dark matter, together accounting for $\rho_m \sim 0.2\rho_c$. If no other from of energy density were present, this would imply that $\Omega \sim 0.2$ and that the universe has an open geometry. However, based on the expectation that the universe was flat (see § 1.1.3 below), Einstein's cosmological constant was reintroduced [44–46] to have $\Omega = 1$. Evidence of a cosmological constant (now also called *dark energy*) came from supernovae data [47,48]. It was shown that the universe is currently in accelerated expansion, exactly what happens if the cosmological energy density is dominated by dark energy. Moreover, after COBE identified the tiny temperature variations in the CMB, many more experiments followed. In particular, the WMAP satellite [49] collected data on the CMB precise enough to confirm that a flat geometry was favored.

1.1.3 Inflation

With the successes of BBN and CMB another mystery arose. Because the universe contains a minimal amount of matter, it means that Ω is non-zero today, and must have been very close to unity in the past. More specifically, it was argued that if $1-\Omega < 0.9$ today, then $1-\Omega < 10^{-16}$ at the time of nucleosynthesis [50]. Moreover, the detection of the CMB suggests that the photons are in thermal equilibrium across the full sky at the time of decoupling. However, in the Hot Big Bang model there are about 10^4 causally disconnected regions that have not had enough time to interact and reach thermal equilibrium. So, why is the universe so similar everywhere? It seemed that either a lot of fine-tuning was required in the initial conditions, or the presence of new physics.

These problems motivated Guth [51] to propose *cosmological inflation*[4]: a period of exponentially accelerated expansion in the very early universe. During inflation $1 - \Omega$ quickly decays, and moreover, causally connected regions become exponentially larger. In other words, the seemingly fine-tuned initial conditions would be a natural consequence of inflation. However, soon it was realized [52,53] that his model did not allow for a smooth transition to a FLRW universe. A new type of inflationary scenario was introduced by Linde [54] and by Albrecht and Steinhardt [55], which did not suffer from the so-called 'graceful exit problem'. Analyses of quantum effects[5] followed [58–61] and showed that inflation also generates small density inhomogeneities. Inflation could provide the seeds of structure formation!

In light of this major success, the paradigm of inflation was embraced. Finally, Linde [62] discovered that a stage of inflation would naturally occur for a broad class of scalar potentials. This is called *chaotic inflation*, whose mechanism is discussed in more detail in § 1.2. The idea that inflation could serve as the origin of structure was so exciting that theorists tried to embed it in the cosmological model (see the discussion on dark energy § 1.1.2). Compelling evidence for inflation came with the observations of the WMAP satellite [49].

This completes the picture of ΛCDM cosmology: an expanding flat universe filled with dark energy, cold dark matter, baryonic matter, neutrinos and radiation. This is complemented by scale-free initial conditions for structure formation. A period of inflation could account for these initial seeds. After inflation ends, its energy density has to be transferred to the Standard Model particles, after which the Hot Big Bang starts.

1.1.4 What's next?

Fast forward to today. Many more precision tests have been performed and confirmed the predictions of ΛCDM. The baseline model, parameterized by only six parameters, works surprisingly well. The current best-fit values of the density parameters of dark energy, dark matter, baryonic matter derived from the CMB are [63]

$$\Omega_\Lambda^0 = 0.692 \pm 0.012, \quad \Omega_c^0 h^2 = 0.1186 \pm 0.0020, \quad \Omega_b^0 h^2 = 0.02226 \pm 0.00023 \ .$$

[4] For more details on the development of inflation, see [3]

[5] In fact the road had been paved earlier by the quantum perturbation analysis of Mukhanov and Chibisov [56] for Starobinky's model [57] of the primordial universe. Also from the English translation, which can be found in [4], they already understood that a phase of cosmological expansion can create the seeds for galaxy formation.

Here the superscript 0 means that the density parameter is evaluated at the present time. The parameter h equals the value of the Hubble parameter in particular units, it is defined in Eq. 1.5. In addition, there are neutrinos and radiation, but today their contribution to the energy density is very small. Radiation did, however, dominate the energy budget at earlier times. Moreover, the value of the Hubble parameter at the present time has the best-fit value (from the CMB)

$$H_0 \equiv 100h \frac{\text{km}}{\text{s Mpc}} = 67.81 \pm 0.92 \ \frac{\text{km}}{\text{s Mpc}} \ . \tag{1.5}$$

In addition, two well-constrained assumptions of ΛCDM are the flatness of the universe and the homogeneity and isotropy of the universe.

The success of ΛCDM is fantastic in the light of observational data. However, we have no clue about the nature of dark matter, dark energy and what drives inflation. More optimistically speaking, perhaps we are on the verge of another radically new idea. For instance, some tensions between datasets are reported [64–66], which might provide us with some hints. And of course the next generation of CMB experiments [67] and large scale structure surveys [68, 69] are designed to reach unprecedented precision with the aim to discover new physics.

The remainder of the thesis is dedicated to scientific questions related to inflation. Broadly speaking, we aim to improve our understanding of which signals to look for and what we can learn about inflation from observations in the near future.

1.2 Inflation

We review some relevant elements of inflation, as it is the main topic of this thesis. We start with a recap of single-field inflation. In particular, we outline the generic mechanism of chaotic inflation in § 1.2.1 and the generation of perturbations in § 1.2.4. Two important ingredients are the slow-roll approximation and mode freezing at horizon crossing. Mode freezing connects inflation naturally to the late universe. It results in the observed 'phase coherence' of the CMB, which is the most compelling evidence in favor of inflation, as we will discuss in § 1.2.5.

Interestingly, the inflationary predictions are sensitive to the details of the field theory under consideration (see § 1.2.4 and § 1.3). Inflation is therefore

the crossroad where particle physicists and cosmologists meet, and precision cosmological observations might reveal a glimpse of high-energy physics. We discuss the theoretical targets in § 1.2.4 and summarize the outline of future observations that might help us to reveal the nature of inflation in § 1.2.6. Finally, we outline the scope of this thesis in § 1.3.

1.2.1 Chaotic inflation

Inflation is a period of accelerated expansion in the early universe. How do we meet the requirements from § 1.1.3 that it solves the fine-tuning problems, but also has a graceful exit to a FRLW universe? To achieve the former it turns out that we need at least 60 efolds of inflation (see e.g. [70]). One efold is the time in which the universe expands by a factor of e, so after N efolds the scale factor grows with a factor e^N. In other words: $dN = d\ln a = Hdt$ (see the discussion following Eq. 1.2).

One thing that comes to mind is a slowly varying cosmological 'constant', or $\dot{H} \approx 0$. Linde [62] figured out that this can be realized with a simple scalar field theory, where the scalar field slowly rolls down to the minimum of its potential, providing a source of almost constant energy density. Importantly, in these models inflation is an *attractor* solution and will eventually happen for a wide range of initial conditions, which explains the name *chaotic inflation*. Let's see how this works.

We consider the toy model of a simple scalar field φ minimally coupled to Einstein gravity

$$S = -\frac{1}{2}\int \sqrt{-g}\left[-M_p^2 R + g^{\mu\nu}\partial_\mu\phi\partial_\nu\phi + 2V(\phi)\right], \tag{1.6}$$

Here R is the Ricci scalar of spacetime. The potential is a smooth function of ϕ with minimum $V(\phi_0) = 0$. Without loss of generality we can take $\phi_0 = 0$. For instance, one could thing of a quadratic potential $V = \frac{1}{2}m^2\phi^2$. The dynamics of the homogeneous scalar field is determined by its equations of motion

$$\ddot{\phi} + 3H\dot{\phi} + V_\phi = 0, \tag{1.7}$$

where we denote a derivative with respect to ϕ with a subscript $V_\phi \equiv \frac{\partial V}{\partial\phi}$, together with the Friedmann equations

$$3H^2M_p^2 = \frac{1}{2}\dot{\phi}^2 + V\ , \tag{1.8}$$

$$\dot{H} = -\frac{\dot{\phi}^2}{2M_p^2}\ . \tag{1.9}$$

The field equation is the same as that of a damped harmonic oscillator, where the Hubble friction depends on the dynamics of the field itself. The second Friedmann equation Eq. 1.9 is not an independent equation, but will be useful in § 1.2.3. Qualitatively, the friction is large when the scalar field is far from the origin, and it gets even larger when the initial velocity $\dot{\phi}$ is substantial. The friction quickly slows down the scalar field, such that it approximately follows the *gradient flow* [54, 55]

$$3H\dot{\phi} + V_\phi \approx 0 \ . \tag{1.10}$$

Assuming that we can neglect the contribution of the kinetic energy to the Hubble friction in Eq. 1.8, the gradient flow approximation becomes (in efolds)

$$\frac{d\phi}{dN} \approx -\frac{M_p^2 V_\phi}{V} \ . \tag{1.11}$$

This shows that the field displacement is small within one expansion time, as long as $V \gg M_p|V_\phi|$. In that case, the potential energy is slowly varying, and the kinetic energy is indeed negligible. This implies that the Hubble parameter is almost constant, and the scale factor grows quasi-exponentially fast for many efolds. This is exactly as desired! Finally, we have to check the validity of the gradient flow approximation. Using Eq. 1.11 we see that we can neglect the field acceleration in Eq. 1.7 if in addition $V \gg M_p^2|V_{\phi\phi}|$.

To prove the attractor behavior of chaotic inflation one has to do a more careful stability analysis. For a nice treatment see for instance [4]. In this thesis we will instead review an argument using the Hamilton-Jacobi formulation in § 1.2.3. Moreover, we assume a homogeneous scalar field from the start. For recent studies of the attractor behavior of scalar field inflation with inhomogeneous initial conditions see [71, 72], see also the review [73].

1.2.2 Slow-roll inflation

An important feature of chaotic inflation is that the scalar field quickly approaches the gradient flow. Tracing it back to the original requirement of accelerated expansion, this ensures that the Hubble parameter is slowly changing in time $-\frac{\dot{H}}{H^2} \ll 1$. Therefore, the gradient flow approximation can be formalised as the *Hubble slow-roll approximation* [74–76]. Slow-roll inflation is defined as a period of near-exponential expansion for which all Hubble slow-roll parameters are much smaller than unity

$$\epsilon \equiv -\frac{\dot{H}}{H^2}, \quad \epsilon_{n+1} \equiv \frac{\dot{\epsilon}_n}{H\epsilon_n} \quad \text{for} \quad n \geq 2 \ . \tag{1.12}$$

Here it is understood that $\epsilon = \epsilon_1$. Usually, the second slow parameter is denoted by $\eta = \epsilon_2$. Notice that in the toy model of § 1.2.1 we could also have rephrased the gradient flow assumption in terms of conditions on potential slow-roll parameters $\epsilon_V \sim \frac{M_p^2}{2}\left(\frac{V_\phi}{V}\right)^2 \ll 1$ and $\eta_V \sim \frac{M_p^2}{2}\frac{V_{\phi\phi}}{V} \ll 1$. However, the Hubble slow roll approximation applies to a much more general class of inflationary models, including many models of multi-field inflation[6]. For that reason we will use the Hubble slow-roll parameters, defined in Eq. 1.12, in the remainder of this thesis.

1.2.3 Hamilton-Jacobi formulation

A particularly neat way to show linear stability of slow roll inflation is presented by Salopek and Bond [74], see also [76]. They employ the Hamilton-Jacobi formulation [74, 77, 78] of single field inflation. Moreover, this formalism can be used to construct inflationary models with exact solutions.

In the Hamilton-Jacobi formalism the scalar field itself[7] parameterizes the inflationary trajectory, and the Hubble parameter $H(\phi)$ determines the inflationary dynamics. The Hubble parameter replaces the potential as fundamental input function and straightforwardly gives all slow-roll parameters (combining Eq. 1.12 and Eq. 1.14)

$$\epsilon \equiv 2M_p^2\frac{H_\phi^2}{H^2}, \quad \epsilon_{n+1} \equiv -2M_p^2\frac{\epsilon_{n,\phi}H_\phi}{\epsilon_n H} \quad \text{for} \quad n \geq 2\ . \tag{1.13}$$

The potential and the Hubble parameter are related through the Hamilton-Jacobi equation, though. This allows us to prove linear stability of chaotic inflation. In addition, this formalism can be used to (locally) reconstruct the potential, given the Hubble slow-roll parameters that characterise the observations (see § 1.2.4).

[6] In a multi-dimensional field space the inflationary trajectory is in general not aligned with the gradient of the potential. Therefore, it makes no sense to use the gradient of the potential as a proxy of the size of the field velocity.

[7] The only requirement is that ϕ is monotonic. This means that, for instance, oscillations around the minimum of the potential cannot be captured within this approach.

Hamilton-Jacobi equation

An easy way to derive the Hamilton-Jacobi equation is to replace $H(t)$ with $H(\phi)$ and use the second Friedmann equation Eq. 1.9 to write

$$\dot{H} = \dot{\phi} H_\phi = -\epsilon H^2 = -\frac{\dot{\phi}^2}{2M_p^2} \quad \longrightarrow \quad -2M_p^2 H_\phi = \dot{\phi} \ . \tag{1.14}$$

This allows us to rewrite the first Friedmann equation Eq. 1.8 as the Hamilton-Jacobi equation

$$V = 3H^2 M_p^2 - 2M_p^4 H_\phi^2, \tag{1.15}$$

where all functions now explicitly depend on ϕ. Given some Hubble parameter $H(\phi)$, the potential follows straightforwardly from the Hamilton-Jacobi equation. If we take the field derivative of Eq. 1.15 and use Eq. 1.14 we find the field equation of motion Eq. 1.7. This means that the Hamilton-Jacobi equation is equivalent to the field equation of motion, modulo some integration constant ϕ_0. The initial value of the Hubble parameter is the same as specifying $\dot{\phi}_0$ at some ϕ_0.

Stability of slow-roll inflation

We now review the stability argument presented by Salopek and Bond [74]. Let's assume that we identified a solution $H(\phi)$ to Eq. 1.15 for a given potential. This is possible in the regime where ϕ is monotonic. It follows directly from perturbing Eq. 1.15, while keeping the potential fixed, that a small perturbation in H evolves as

$$\delta H(\phi) = \delta H(\phi_0) \exp\left(\int_{\phi_0}^{\phi} d\phi \ \frac{3}{2M_p^2} \frac{H}{H_\phi} \right) \ . \tag{1.16}$$

Since $\dot{\phi}$ and $\frac{H}{H_\phi}$ have opposite sign the perturbations will decay. To understand how fast they decay rewrite the argument of the exponent in terms of efolds by using $d\phi = \frac{\dot{\phi}}{H} dN = -2M_p^2 \frac{H_\phi}{H} dN$. This yields

$$\delta H(N) = \delta H(0) \exp\left(-3N\right) \ . \tag{1.17}$$

We learn that different solutions $H(\phi)$ of Eq. 1.15 approach each other exponentially fast. Therefore, any functional form of $H(\phi)$ provides an (possibly non- inflationary) linear attractor solution to the corresponding potential, computed from Eq. 1.15, as long as it is monotonic.

To address the attractor behavior of chaotic inflation, let's make use of the slow roll expansion. The zeroth order solution (with $\epsilon = 0$) for the Hubble

parameter is given by $H_{\rm SR}^2 = \frac{V}{3M_p^2}$. The solution $H(\phi)$ to the Hamilton-Jacobi equation is always larger than this, but to support inflation it has to obey

$$H_{\rm SR} < H(\phi) < \sqrt{\frac{3}{2}} H_{\rm SR} \ . \tag{1.18}$$

Therefore, is there a solution close to $H_{\rm SR}$? If yes, it can be found perturbatively from Eq. 1.15

$$H^{(0)} = H_{\rm SR}, \quad H^{(1)} = H_{\rm SR}\sqrt{1 + \tfrac{1}{3}\epsilon^{(0)}}, \tag{1.19}$$

etcetera. Therefore, we expect that if the slow-roll parameters computed with $H_{\rm SR}$ are small, then the solution to Eq. 1.15 is an inflationary solution, and moreover it is an attractor. In other words, slow-roll inflation is an attractor. Please see [76] for a more precise treatment.

Reconstruction potential

The Hamilton-Jacobi formalism can also be used to find exact inflationary solutions [75, 77, 79, 80]. To illustrate this, we reconstruct the potential which allows for slow roll parameters of the form

$$\epsilon = \frac{p}{2\Delta N + p} \ , \tag{1.20}$$

where $\Delta N = N_e - N$ is the number of efolds before the end of inflation. We added a p in the denominator to ensure that $\epsilon = 1$ at the end of inflation. Notice that with this parameterization all other slow-roll parameters follow automatically. This parameterization of ϵ has to be understood as a fit to the data, i.e. it only is guaranteed to work well at the time that the observable modes cross the horizon (see § 1.2.4). Therefore, the potential we reconstruct provides a good approximation around the field values of horizon crossing only.

First, we write ϵ in terms of ϕ by integrating $d\phi/dN = -\sqrt{2\epsilon}M_p$. Here the minus sign is our choice of convention. This yields $\epsilon = \frac{2M_p^2 p^2}{\phi^2}$. From Eq. 1.13 it then follows that $H = c\phi^p$, with c some constant. Therefore, we find the following potential from the Hamilton-Jacobi equation Eq. 1.15

$$V = 3c^2 M_p^2 \phi^{2p-2}\left(\phi^2 - \frac{2p^2 M_p^2}{3}\right) \ . \tag{1.21}$$

These are the familiar power law potentials up to a small correction, which is only there to ensure the exact behavior of the assumed slow roll parameters. One can indeed check that $\dot\phi = Hd\phi/dN = -2cpM_p^2\phi^{p-1}$ solves the field

equations of motion exactly.

One might worry that if we slightly change the functional form of $H(\phi)$ around horizon crossing, this could change the global structure of the potential quite a bit. However, in single field slow roll inflation this will not affect the inflationary predictions, so long the slow parameters behave smoothly. Therefore, we should not take the global behavior of the resulting potential too seriously, except possibly when the form of $H(\phi)$ is constrained by symmetries.

1.2.4 Inflation as the origin of structure

The major success of inflation is that it provides a mechanism to create the initial seeds for structure formation from quantum fluctuations [56]. The rough picture is that quantum perturbations are stretched exponentially fast during inflation. The Hubble scale $\frac{1}{aH}$ quickly drops below their comoving wavelengths, where their amplitude freezes out. At much later times, when they become sub-Hubble again, they provide the gravitational wells that triggers structure formation.

Primordial perturbations

Let us recap the main steps in the computation of primordial perturbations for single field slow roll inflation. We follow the treatments of [5, 81, 82], albeit with a different notation. The leading order behavior of quantum fluctuations is captured by a linear perturbation analysis. Therefore, we start with linear perturbations around the homogeneous inflationary background solution. Using the ADM decomposition of the metric [83] we write

$$\phi(t, \mathbf{x}) = \phi(t) + \delta\phi(t, \mathbf{x}), \tag{1.22a}$$

$$ds^2 = -\mathcal{N}dt^2 + g_{ij}\left(dx^i + \mathcal{N}^i dt\right)\left(dx^j + \mathcal{N}^j dt\right) \tag{1.22b}$$

align Here $\mathcal{N}(t, \mathbf{x})$ and $\mathcal{N}_i(t, \mathbf{x})$ are the lapse and the shift functions, respectively. They are not dynamical, but auxiliary variables solved by the Einstein equations, which become constraints in this case. The remaining perturbations in the metric can be decomposed into scalar, vector and tensor modes, depending on how they transform under rotations about the axis defined by its Fourier vector $\mathbf{k}$. This decomposition is quite useful because the different types of perturbations decouple at the linear level, as a consequence of translational and rotational invariance of the background [5]. The spatial metric perturbation g_{ij} together with the field perturbation can be split in two scalar, one vector and one tensor mode. However, not all of them are physical degrees of freedom, since reparametrization invariance $x^\mu \to x^\mu + \xi^\mu(t, \mathbf{x})$, removes one

scalar and one vector mode. Therefore, we are left with one scalar and one tensor mode, equivalent to one scalar and two tensor degrees of freedom. For the purpose of the computation it is useful to work in a particular gauge that fixes time and spatial reparametrizations. We choose the *comoving gauge*

$$\delta\phi = 0 \quad \text{and} \quad g_{ij} = a^2(t)\left((1+2\mathcal{R})\delta_{ij} + h_{ij}\right), \tag{1.23}$$

where $\mathcal{R}$ is the *comoving curvature perturbation* which measures the curvature of the spatial hypersurfaces in this gauge. Moreover, h_{ij} is transverse and traceless and contains the two tensor degrees of freedom. The quadratic action for $\mathcal{R}$ and h_{ij} can be found by expanding the full action Eq. 1.6 to second order, replacing $\mathcal{N}$ and $\mathcal{N}^i$ by their solution of the constraint equations, and performing integration by parts

$$S^{(2)} = \int d^4x a^3 M_p^2 \left[\epsilon\left(\dot{\mathcal{R}}^2 - \frac{1}{a^2}(\nabla\mathcal{R})^2\right) + \frac{1}{8}\left(\dot{h}_{ij}^2 - \frac{1}{a^2}(\nabla h_{ij})^2\right)\right] . \tag{1.24}$$

To perform the quantization of the curvature perturbations, it is convenient to go to conformal time $ad\tau = dt$ and change to the canonically normalized Mukhanov-Sasaki variable [84–86]

$$v \equiv z\mathcal{R}M_p \quad \text{with} \quad z \equiv a\sqrt{2\epsilon} . \tag{1.25}$$

The quantization of the theory [87] proceeds by promoting the field v to a quantum operator

$$\hat{v}(t,\mathbf{x}) = \int \frac{d^3\mathbf{k}}{(2\pi)^3}\left[v_k(\tau)\hat{a}_\mathbf{k}e^{i\mathbf{k}\cdot\mathbf{x}} + v_k^*(\tau)\hat{a}_\mathbf{k}^\dagger e^{-i\mathbf{k}\cdot\mathbf{x}}\right], \tag{1.26}$$

where the creation and annihilation operators satisfy the commutation relations

$$\left[\hat{a}_\mathbf{k}, \hat{a}_\mathbf{p}^\dagger\right] = (2\pi)^3\delta_D(\mathbf{k}-\mathbf{p}), \quad [\hat{a}_\mathbf{k}, \hat{a}_\mathbf{p}] = \left[\hat{a}_\mathbf{k}^\dagger, \hat{a}_\mathbf{p}^\dagger\right] = 0 . \tag{1.27}$$

This, together with the selection of the Bunch-Davies vacuum $\hat{a}_\mathbf{k}|0\rangle = 0$, fixes the initial conditions of the mode functions $v_k(\tau)$. The mode functions satisfy a modified Klein-Gordon equation in conformal time

$$v_k'' + \left(k^2 - \frac{z''}{z}\right)v_k \tag{1.28}$$

In the short wavelength limit $k^2 \gg \frac{z''}{z}$ this is the equation of a harmonic oscillator. In the long wavelength limit $k^2 \ll \frac{z''}{z}$ one of the solutions is $v_k \sim z$, which corresponds to $\mathcal{R} \sim$ const. This agrees with the homogeneous equation

of motion $\partial_t(a^3\epsilon\dot{\mathcal{R}}) = 0$, derived from the quadratic action Eq. 1.24. The constant solution is the dominant one, as long as $\int \frac{dt}{a^3\epsilon}$ is decaying. For slow-roll inflation this is always the case.

More precisely, at first order in slow-roll, the solution of the mode function to Eq. 1.28 subject to the quantum initial conditions is given by

$$v_k(\tau) = \sqrt{\frac{\pi}{4k}}\sqrt{-k\tau}H_\nu^{(1)}(-k\tau), \quad \text{with} \quad \nu \equiv \frac{3}{2} + \epsilon - \frac{1}{2}\eta \ , \tag{1.29}$$

modulo a random phase. On *superhorizon scales* $-k\tau = \frac{k}{aH} \ll 1$ the mode function of the curvature perturbation asymptotes to [88]

$$\lim_{-k\tau\ll 1} |k^{3/2}\mathcal{R}_k| = \frac{2^\nu\Gamma(\nu)}{\sqrt{8\pi\epsilon}}\frac{H}{M_p}(-k\tau)^{3/2-\nu} \ . \tag{1.30}$$

Using the approximate relation [82] that for slow-roll inflation $\frac{H}{M_p\sqrt{\epsilon}}(-k\tau)^{3/2-\nu}$ is a constant, this allows us to evaluate Eq. 1.30 at *horizon crossing* $-k\tau = \frac{k}{aH} = 1$ where $\nu \approx 3/2$. This validates the *horizon crossing formalism*, where the typical size of curvature perturbations at the end of inflation is related to the inflationary background quantities evaluated at horizon crossing.

The variance of curvature perturbations is captured by the dimensionless power spectrum $\Delta^2_{\mathcal{R}}(k)$, defined as

$$\frac{k^3}{2\pi^2}\langle\mathcal{R}(\mathbf{k})\mathcal{R}(\mathbf{k}')\rangle \equiv (2\pi)^3\delta_D^{(3)}(\mathbf{k}+\mathbf{k}')\Delta^2_{\mathcal{R}}(k) \ . \tag{1.31}$$

Homogeneity and isotropy imply that the correlation functions in Fourier space always come with an overall delta-function. Using Eq. 1.30 the dimensionless power spectrum evaluates to

$$\Delta^2_{\mathcal{R}}(k) = \left.\frac{H^2}{8\pi^2\epsilon M_p^2}\right|_{k=aH} \ . \tag{1.32}$$

Since H and ϵ are nearly constant during slow-roll inflation, the power spectrum is almost scale-invariant. It has a small scale dependence though, because different modes cross the horizon at different times and they will all feel a different Hubble and slow-roll parameter. Therefore it is convenient to parameterize the power spectrum by its amplitude A_s and *scalar spectral index* n_s

$$\Delta^2_{\mathcal{R}}(k) = A_s(k_*)\left(\frac{k}{k_*}\right)^{n_s-1} \ . \tag{1.33}$$

Here k_* is the 'pivot scale', a reference scale at which the amplitude is evaluated.

A similar analysis applies to the tensor perturbations [57]. The transverse and traceless h_{ij} contains two tensor polarization modes. Comparing the relative normalizations of h_{ij} and $\mathcal{R}$ in the quadratic action Eq. 1.24 we expect the power spectrum of tensor perturbations Δ_t^2 to be $2 \times 8\epsilon \times \Delta_{\mathcal{R}}^2$, which is indeed the case:

$$\Delta_t^2(k) = \left.\frac{2H^2}{\pi^2 M_p^2}\right|_{k=aH} . \tag{1.34}$$

Also the power spectrum of tensor perturbations can be parametrized in terms of the *tensor spectral index* n_t and the *tensor-to-scalar-ratio* r

$$\Delta_t^2(k) = A_t(k_*)\left(\frac{k}{k_*}\right)^{n_t} \quad \text{and} \quad r(k_*) \equiv \frac{A_t(k_*)}{A_s(k_*)} . \tag{1.35}$$

The tensor-to-scalar-ratio measures the ratio between the amplitude of tensor perturbations with respect to the scalar perturbations.

Theoretical Targets - First of all, a measurement of stochastic background of primordial gravitational waves on large scales would be groundbreaking, as it probes the quantum nature of gravity. Moreover, it provides another important confirmation of inflation and probes its energy scale. For instance, for the simplest models of inflation[8] a measurement of both the scalar amplitude A_s and the tensor-to-scalar ratio r is translated into $V^{1/4} \sim \left(\frac{r}{0.009}\right)^{1/4} \times 10^{16}$ GeV [89]. It has been argued [67] that $\sigma(r) = 0.001$ is a clear theoretical benchmark, because it allows us to falsify all simple models that naturally explain the observed spectral tilt.
Moreover, using the slow-roll approximation, we can summarize the leading order predictions of the simplest models of inflation as

$$r = 16\epsilon, \quad n_s = 1 - 2\epsilon - \eta, \quad n_t = -2\epsilon . \tag{1.36}$$

Notice the *consistency relation* $r = -8n_t$ [75]. This provides us with another theoretical target: a violation of this consistency relation signals that we should break at least one of the conditions listed in footnote 8.

At this stage it is perhaps interesting to remark that, going beyond the simplest realization of inflation, the curvature perturbations could have a sound

[8] By the simplest models of inflation we mean canonical single-field slow-roll inflationary models minimally coupled to gravity, and with Bunch-Davies initial conditions.

speed c_s smaller than unity, see e.g. [90]. The quadratic action for curvature perturbations now reads

$$S^{(2)} = \int d^4x a^3 M_p^2 \left[\epsilon \left(\frac{\dot{\mathcal{R}}^2}{c_s^2} - \frac{1}{a^2} (\nabla \mathcal{R})^2 \right) \right] . \tag{1.37}$$

Repeating similar computations as outlined above yields $r = 16\epsilon c_s$, assuming that $c_s \approx$ const. In other words, this might change our interpretion of the data. In Chapter 5 we will illustrate how this effect may arise in a simple two field set-up, where the curvature perturbation interacts with a heavy degree of freedom.

Primordial non-Gaussianities

We have seen that single field inflation generates scalar and tensor perturbations. Above we only computed their variance, but in principle the full probability distribution could be computed. Primordial non-Gaussianities have been studied thoroughly since the pioneering works [81,91], see e.g. [92,93] for reviews. Since the computation of primordial perturbations is organized perturbatively, it is natural to work with correlation functions. In this thesis we consider only the two- and three-point correlation functions. The bispectrum of curvature perturbation is defined by

$$\langle \mathcal{R}(\mathbf{k}_1) \mathcal{R}(\mathbf{k}_2) \mathcal{R}(\mathbf{k}_3) \rangle \equiv (2\pi)^3 \delta_D^{(3)}(\mathbf{k}_1 + \mathbf{k}_2 + \mathbf{k}_3) B_{\mathcal{R}}(k_1, k_2, k_3) . \tag{1.38}$$

A similar definition applies to the tensor perturbations and any cross-correlation between the variables. The dimensionless bispectrum and shape function are given by

$$\mathcal{I}_{\mathcal{R}}(k_1, k_2, k_3) \equiv \frac{k_1^2 k_2^2 k_3^2}{4\pi^4} B_{\mathcal{R}}(k_1, k_2, k_3), \tag{1.39a}$$

$$f_{NL}(k_1, k_2, k_3) \equiv \frac{5}{6} \frac{B_{\mathcal{R}}(k_1, k_2, k_3)}{P_{\mathcal{R}}(k_1) P_{\mathcal{R}}(k_2) + P_{\mathcal{R}}(k_1) P_{\mathcal{R}}(k_3) + P_{\mathcal{R}}(k_2) P_{\mathcal{R}}(k_3)} , \tag{1.39b}$$

respectively. The denominator of the shape function depends on the dimensionfull power spectrum $P_{\mathcal{R}}(k) \equiv \frac{2\pi^2}{k^3} \Delta^2_{\mathcal{R}}(k)$. The full scale dependence of the bispectrum for canonical single field slow-roll inflation has been computed for the first time by Maldacena [81]. It turns out that the amplitude of the signal is very small, because interaction terms are slow-roll suppressed $f_{NL} \sim \mathcal{O}(\epsilon, \eta)$.

The bispectrum contains a wealth of information. If we constrain or probe its amplitude and its three dimensional scale-dependence, we learn about the possible (self-)interactions of the inflaton. More sizeable non-Gaussianities $f_{NL} \sim 1$ might be generated if we deviate from one of the assumptions of

canonical single-field slow-roll inflation with Bunch-Davies initial conditions. However, please keep in mind that a bispectrum with amplitude of order unity is already extremely challenging to measure, since the amplitude of the power spectrum is tiny $\Delta^2_{\mathcal{R}} \sim 10^{-9}$ (see § 1.2.5), implying that $\mathcal{I}_{\mathcal{R}} \sim 10^{-18} f_{NL}$. But this is definitely worth pushing for.

The bispectrum is a three-dimensional function, which makes it challenging to compare efficiently with data. Also, the scale-dependence cannot always be computed analytically for a given inflationary model. In order to compare with the data, it is therefore useful to have a set of templates that resemble various possible scale-dependencies of the bispectrum well. Let us highlight three well-motivated shape templates for the bispectrum:

- *The local shape.* A simple modification to the Gaussian probability distribution function (in real space) arises from a small non-linear correction to the Gaussian curvature perturbation [94]

$$\mathcal{R}(\mathbf{x}) = \mathcal{R}_g(\mathbf{x}) + \frac{3}{5} f_{NL}^{\rm loc} \left(\mathcal{R}_g^2(\mathbf{x}) - \langle \mathcal{R}_g^2(\mathbf{x}) \rangle \right) \ . \tag{1.40}$$

  This corresponds to a constant shape function equal to $f_{NL}^{\rm loc}$. This explains why f_{NL} is defined as it is. The factor $3/5$ comes from the translation to the primordial gravitational potential, see § 1.4. The dimensionless bispectrum, on the other hand, peaks in the *squeezed configuration* where one of the wavenumbers is much smaller than the others $k_1 \ll k_2, k_3$. This type of non-Gaussianity arises for instance in multi-field inflation [95], where the curvature perturbations are sourced on super-Hubble scales by the other fields. For a nice explanation and a review of other scenarios that create local non-Gaussianities see [96].

- *The equilateral shape.* The dimensionless bispectrum of equilateral non-Gaussianity peaks in the equilateral configuration where all wavenumbers are equal $k_1 = k_2 = k_3$.

$$\mathcal{I}^{\rm eq}_{\mathcal{R}}(k_1, k_2, k_3) = \frac{6}{5} f^{\rm eq}_{NL} \frac{81 \Delta^2_{\mathcal{R}}}{(2\pi^2)^4} \frac{k_1 k_2 k_3}{K^3}, \quad \text{with} \quad K \equiv k_1 + k_2 + k_3 \ . \tag{1.41}$$

  Equilateral non-Gaussianity is generated in models of inflation where the interactions are most important around the time of horizon crossing. For instance it is created in single field inflation with a small inflaton sound speed [97–99].

- *The quasi-single-field shape.* Finally, if the inflaton interacts with an isocurvaton of mass $\mu \lesssim H$ a bispectrum with a shape that interpolates

between local and equilateral is produced [100,101]. Its scale dependence is well approximated by the following template

$$\mathcal{I}^{\rm qsf}_{\mathcal{R}}(k_1,k_2,k_3)=\frac{6}{5}f^{\rm qsf}_{NL}\frac{9\sqrt{3}\Delta^2_{\mathcal{R}}}{(2\pi^2)^4}\frac{k_1k_2k_3}{K^3}\frac{N_\nu(8\kappa)}{\sqrt{\kappa}N_\nu(8/27)}, \tag{1.42}$$

with $\kappa\equiv k_1k_2k_3/K^3$ and N_ν the Neumann function of order $\nu\equiv\sqrt{\frac{9}{4}-\frac{\mu^2}{H^2}}$.

Theoretical targets - Which precision do we require from future observations, such that we learn something even in the absence of a detection? Concerning the amplitude of these three shapes, the theoretical benchmark for equilateral non-Gaussianity reads $\sigma(f^{\rm eq}_{NL})=\mathcal{O}(1)$. First of all, single-field slow-roll inflation necessarily produces an amplitude smaller than unity [97]. Second, a detection of $f^{\rm eq}_{NL}$ larger than unity implies that inflation becomes strongly coupled, or it signals the presence of new fields [102–104]. The theoretical benchmarks for the other two shapes are less clear. In [103] it has been argued that $\sigma(f^{\rm loc}_{NL})=\mathcal{O}(1)$ is of theoretical interest, because this can disfavor a particular class of inflationary models.

A very important target for future observations is to constrain the amplitude of the bispectrum in the *squeezed configuration*, where one the wavenumbers is much smaller than the others. Maldacena [81] derived an important *consistency relation* of the single field bispectrum

$$B^{\rm sq}_{\mathcal{R}}(q,k_s)\equiv\lim_{q\ll k_s}B_{\mathcal{R}}(q,k_s,k_s)=(1-n_s(k_s))P(q)P(k_s)\ . \tag{1.43}$$

This relation was proven to be valid for all single-field attractor models of inflation [105–107]. Moreover, it was shown to be non-observable [108,109] in the late universe, up to projection effects. In terms of the shape function one gets[9]

$$f^{\rm sq,\ obs}_{NL}(q,k_s)=0+\mathcal{O}\left((q/k_s)^2\right) \tag{1.44}$$

Therefore, any detection of a signal in the squeezed limit would rule out single field inflation!

[9] The reason is that a local observer is freely falling in a FRLW background modified by the long wavelength perturbation $\mathcal{R}_\ell$. It turns out that the observer can only distinguish $\mathcal{R}_\ell$ from the background by its second spatial derivative (or higher) [110].

Initial conditions after inflation

After inflation ends, its energy density is transferred into a soup of particles that lead to the universe today. This process is called reheating, and its precise mechanism is unknown. After many interactions in this dense plasma it is expected that the baryons, photons and neutrinos thermalize. This is the onset of the Hot Big Bang.

The reason why we can probe the epoch of inflation, regardless of the details of reheating and other unknown physics, is due to an important theorem by Weinberg [111]. It states that the curvature perturbation $\mathcal{R}$ remains conserved on superhorizon scales whenever perturbations are adiabatic, independent of the matter content of the universe. Only when the curvature perturbations enter the horizon, they start to evolve again. This allows us to probe the primordial universe by observing the largest scales we can access today.

Adiabatic perturbations are perturbations that mimic a local time shift of the homogeneous background. Perturbations along the inflationary background solution correspond to a local time shift of the homogeneous background. Some parts of the universe end inflation slightly ahead of time and other parts slightly behind, i.e. single field inflation produces adiabatic perturbations. After the inflaton has decayed into the hot plasma, we can relate the overdensities of the various particle species X and Y to each other

$$\delta t = \frac{\delta\rho_Y}{\dot{\rho}_Y} = \frac{\delta\rho_X}{\dot{\rho}_X} \sim \frac{\delta_X}{1+\omega_X} = \frac{\delta_Y}{1+\omega_Y} \ . \tag{1.45}$$

Here we defined the *density contrast* $\delta_X \equiv \frac{\delta\rho_X}{\rho_X}$ and the *equation of state* $\omega_X \equiv p_X/\rho_X$ for each of the particles species X. This implies the following relation between matter, cold dark matter, photon and neutrino overdensities on superhorizon scales

$$\delta_b = \delta_c = \frac{3}{4}\delta_\gamma = \frac{3}{4}\delta_\nu \ . \tag{1.46}$$

Therefore, as long as we understand the evolution of the density perturbations when they enter the horizon, we can relate their statistical properties to those of $\mathcal{R}$. It is most convenient to study perturbations on the largest scales, because i) they only entered the horizon recently, where we understand better the constituents of the universe and ii) they are well captured by linear perturbation theory and carry the cleanest information from the early universe.

1.2.5 Evidence and constraints

The statistics of the CMB temperature variations confirm a couple of non-trivial predictions of inflation. The CMB provides us with a snaphot of the universe when it was only approximately 380.000 years old. This means that we probe, among other things, superhorizon correlations of density fluctuations. This is the reason that it provides an excellent test of inflation. Moreover, the current precision reached by CMB measurements starts to constrain the subtle details of inflation. We summarize the key findings so far:

- The structure of peaks and troughs of the CMB power spectrum provides compelling evidence in favor of inflation [112]. To appreciate this idea, we give an extremely simplified explanation of CMB physics, see e.g. [113, 114] for more details. Before the CMB photons were emitted, the photons were tightly coupled to electrons through Thomson scattering. The electrons were, in turn, tightly coupled to protons by the Coulomb interaction. Therefore, the system behaved like a single photon-baryon fluid. This fluid supports 'acoustic oscillations' as a consequence of the competing effects of gravitational collapse and radiation pressure. The gravitational source term is set by the initial conditions provided by inflation. The special feature of inflation is that $\dot{\mathcal{R}} = 0$ on superhorizon scales, which implies that the density perturbations all start oscillating in phase (at maximal amplitude). The acoustic oscillations suddenly stop at recombination when the radiation pressure disappears and the CMB photons start free-streaming towards us. Because the photons have to climb out of the potential wells created by the matter overdensities, they provide us with a snapshot of the density field at recombination. The density perturbations of a given wavenumber are all captured in the same phase of their oscillation, because they started oscillating at the same time when they entered the horizon. On the largest scales the perturbations are still frozen. On the smaller scales some modes are captured in their minimum, some in their maximum, and this produces the peaks and troughs in the CMB temperature power spectrum. If not for this phase coherence, the peaks in the CMB temperature spectrum would be washed away.

- The CMB probes the primordial power spectrum of curvature perturbations in the range $0.0001\ \text{Mpc}^{-1} \leq k \leq 0.3\ \text{Mpc}^{-1}$. The *Planck* collaboration [115] has reported a detection of the deviation from a scale-invariant power spectrum with 5.6σ confidence level. Moreover, the amplitude is given by $\ln(10^{10} A_s) = 3.089 \pm 0.036$ at $k_* = 0.05\ \text{Mpc}^{-1}$. Joint constraints on the scalar tilt n_s and the tensor-to-scalar ratio r are shown

in Figure 1.2. They are evaluated at the pivot scale $k_* = 0.002$ Mpc^{-1}, which corresponds to a horizon-crossing time between 50 and 60 efolds before the end of inflation [116].

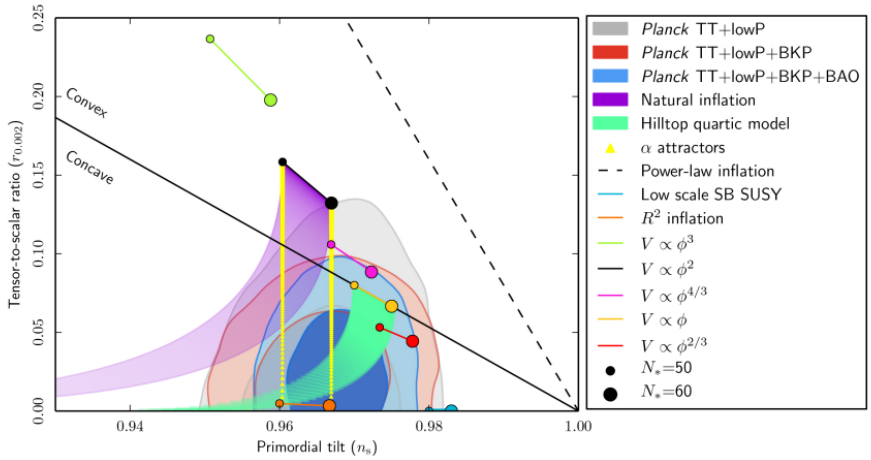

Figuur 1.2: Marginalized joint 68% and 95% CL contours on the tensor-to-scalar ratio r and spectral tilt n_s at the pivot scale $k_* = 0.002$ Mpc^{-1} from *Planck* [115] together with other datasets. The predictions of some selected inflationary models are shown as well.

- Phase coherence puts strong constraints on the adiabaticity of the universe. *Planck* [115] has tested some of the relations in Eq. 1.46 to almost percent level accuracy. A detection would falsify single field slow-roll inflation, and is for that reason very interesting. It is possible that isocurvature (non-adiabatic) perturbations are generated during inflation, but it requires that more than one scalar degree of freedom is excited. Therefore, late-time isocurvature perturbations could give us some information about the mechanism of inflation. However, how the late-time isocurvature perturbations are related exactly to the isocurvature perturbations produced during inflation depends on the details of reheating. In fact, reheating might even wash out (part of) the primordial isocurvature perturbations [117].

- The Gaussianity of the primordial fluctuations has also been tested to a high degree. In the comparison with CMB data [118], various templates for the shape are considered, some of them are described in Eq. 1.40, Eq. 1.41 and Eq. 1.42. The amplitude is evaluated in the equilateral configuration $f_{NL}(k) \equiv f_{NL}(k, k, k)$. The current best constraints [118]

on the local and equilateral types of non-Gaussianity are

$$f_{NL}^{\rm loc} = 0.8 \pm 5.0 \quad \text{and} \quad f_{NL}^{\rm eq} = -4 \pm 43 \quad (68\%\ \text{CL})\ . \tag{1.47}$$

- The location of the first peak in the CMB spectrum depends on the geometry of the universe. This indicates that the universe is flat to very high precision $\Omega_\kappa = -0.005^{+0.016}_{-0.017}$ at 95% CL [115]. This is compatible with inflation, because it was designed to create a flat universe.

1.2.6 Future probes of inflation

What are the observations that will teach us more about inflation in the future?

Cosmic Microwave Background experiments - There is much room for improvement in CMB experiments to constrain the amplitude of primordial tensor fluctuations by observing *primordial B-mode polarization*. The CMB photons are polarized via Thomson scattering, see e.g. [119]. An electron at the last scattering surface is surrounded by a slightly non-isotropic radiation field, because of the small temperature variations. Therefore, the CMB photons will carry an overall polarization that is correlated with the temperature fluctuations. Polarization is a vector field and can be decomposed in so-called E-modes and B-modes [120–122]. This decomposition is particularly useful because *only* tensor perturbations can create a primordial B-mode signal. Therefore, constraining the amplitude of the primordial B-mode polarization is an important observational goal. It has been forecast that CMB-S4 [67] will be able to do better than $\sigma(r) = 0.001$, provided there is large increase in the number of detectors.

Concerning primordial non-Gaussianities, it has been estimated [123] that, with improved temperature and polarization measurements, the error bars can maximally decrease by a factor of two, which is unfortunately not sufficient to reach the theoretical thresholds quoted between Eq. 1.42 and Eq. 1.43. Fortunately, there is a promising opportunity to constrain the squeezed primordial bispectrum from the CMB by observing spectral distortions [124, 125]. The energy spectrum of the CMB is not a perfect blackbody, but has tiny distortions [126]. Two types of spectral distortions are sensitive to the integrated power spectrum between $1\text{Mpc}^{-1} < k < 50\text{Mpc}^{-1}$ [127] and $50\text{Mpc}^{-1} < k < 10^4\text{Mpc}^{-1}$ [126] respectively. Therefore, correlating the spectral distortion with large scale temperature fluctuations provides a measurement of the bispectrum in the ultra-squeezed limit. It has been forecast [128] that a futuristic idealized cosmic-variance-limited survey can reach error bars of order

$\sigma(f_{NL}^{\rm sq}) = \mathcal{O}(10^{-4})$.

Large Scale Structure experiments - Long after the emission of the CMB photons the small initial density perturbations evolved into the large scale structures in which galaxies formed. Galaxies and neutral hydrogen trace the underlying matter distribution, and can be used to infer its statistical properties. Moreover, weak lensing in addition infers the integrated matter density along the line of sight. Since large scale structure surveys help us to reconstruct the three-dimensional distribution of matter, they contain in principle much more information than the two-dimensional CMB. The challenge, however, is to extract this information, because gravitational clustering is a non-linear process. Moreover, since galaxies are expected to form only in the densest regions, they are biased tracers of the matter distribution. In this thesis we consider the possibility of using the bispectrum as a probe of primordial non-Gaussianities (see § 1.3 and § 1.4.) Another opportunity to constrain primordial non-Gaussianities comes from galaxy bias. It turns out that a non-zero squeezed bispectrum imprints a particular scale-dependence in the galaxy power spectrum [129]. The prospects are that Euclid [69] can reach $\sigma(f_{NL}^{\rm sq}) = \mathcal{O}(5)$ [130] and the optimized proposed SPHEREx survey can reach $\sigma(f_{NL}^{\rm sq}) = \mathcal{O}(1)$ [130]. Moreover, future intensity mapping experiments (of neutral hydrogen) such as SKA [131], are expected to be competitive $\sigma(f_{NL}^{\rm sq}) = \mathcal{O}(0.5)$ [132].

Other probes - With the exciting discipline of gravitational-wave cosmology [133], we can search for a stochastic background of primordial gravitational waves directly. From the CMB to ground-based GW experiments, a range of scales with more than 20 orders of magnitude [134] is scanned. This allows us to constrain the tensor tilt n_t to much better accuracy than the CMB alone [134, 135]. Moreover, it constrains the amplitude of primordial gravitational waves and therefore r. Another probe is offered by the non-detection of primordial black holes [136], which constrains the integrated primordial scalar power spectrum.

1.3 Outline thesis

This thesis is about "spectroscopy" of two-field inflation. The power spectrum and bispectrum contain a wealth of information about the primordial universe. In particular, the amplitude and scale dependence of inflationary spectra might tell us something about the spectrum of masses of other fields relevant at the time of inflation, and their couplings to the inflaton.

This thesis consists of two parts. In Part I we study the phenomenology of two-field extensions of the simplest models of inflation. In Part II we investigate the utility of the bispectrum as a probe of non-Gaussianities in large scale structure experiments.

Multi-field inflation

Inflation gives us an opportunity to probe energy scales not accessible at earth based experiments. This means that inflation may shed light on the UV completion of the Standard Model and teach us something about fundamental physics. For instance, string theory typically predicts the presence of many scalar moduli fields [137] which could be active during inflation, and leave their imprint in the data. Being agnostic about the precise UV completion of inflation and the Standard Model, it is important to identify some of its essential features. For instance, when only one light degree of freedom is excited during inflation, the effective field theory of inflation [99] provides the most general way to parametrize our ignorance about the parent theory. However, we eventually would like to interpret the EFT coefficients in terms of properties of the UV embedding, such as extra dimensions, the mass and spin of other fields, higher order kinetic terms, etcetera. Therefore, in general it is important to understand how various classes of inflationary theories affect the low energy dynamics of the inflaton and its possible coupling to other light degrees of freedom.

In Part I of this thesis we will be mainly concerned with two-field inflation as a representative of the inflationary class of multi-field models of the form

$$S = \frac{1}{2}\int d^4x\sqrt{-g}\left[M_p^2 R - G_{ab}(\phi^c)\partial_\mu\phi^a\partial^\mu\phi^b - 2V(\phi^a)\right] . \tag{1.48}$$

Here $G_{ab}(\phi^c)$ is the field metric characterizing the kinetic terms. Moreover, R is the Ricci scalar of spacetime and $V(\phi^a)$ the potential energy density of the scalar fields. The action of perturbations will now contain an extra scalar degree of freedom besides the curvature perturbation: the *isocurvature perturbation*. We study a broad mass spectrum of the isocurvature perturbation,

ranging from massless all the way to heavy with respect to the Hubble scale. Our aim is to improve our understanding about the observational viability and falsifiability of such theories when the isocurvaton and inflaton are coupled to each other. Depending on the coupling strength, the transfer of power from the isocurvature perturbations to the curvature perturbations is either efficient or inefficient. In Figure 1.3 we illustrate the different regimes of parameter space we cover in this thesis.

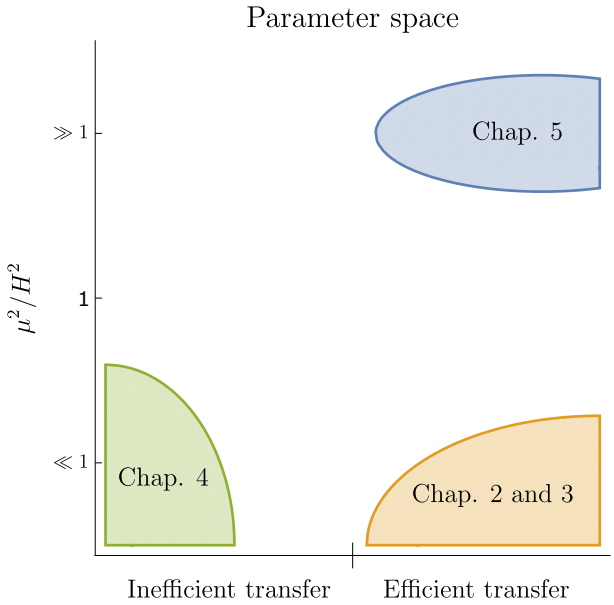

Figuur 1.3: An illustration of the parameter space of two-field inflation covered in Part I of this thesis. On the vertical axis we vary the mass of the isocurvature perturbations (see Eq. 2.13) in units of the Hubble scale μ^2/H^2. The horizontal axis represents the coupling strength between isocurvature and curvature perturbations. It is divided into two regimes. The (left) right part corresponds to (in)efficient transfer of power from the isocurvature perturbations to the curvature perturbations.

- Chapter 2: the first part of this chapter serves as a review of a few selected elements of multi-field inflation. In particular, we recap the kinematical analysis of multi-field inflation and we pay special attention to the definition of the entropy mass (the effective mass of isocurvature perturbations). In turns out that the linear dynamics of two-field inflation is described by only a few kinematical and geometrical parameters. These are the field radius of curvature, the entropy mass and the Hubble slow-roll parameters.
  This motivates us to introduce Orbital Inflation: a family of two-field

models of inflation where all these parameters are (approximately) constant. We discuss their phenomenology, and we highlight a few results in the regime typically not considered in quasi-single field inflation (inflation with additional fields of mass $m \sim H$). First, the larger the coupling to the isocurvature perturbations, the more they become suppressed compared to the curvature perturbations. Second, the value of the isocurvature mass determines how the predictions for n_s shift. This may help to distinguish between various entropy masses. Finally, by means of the Hamilton-Jacobi formalism we locally reconstruct potentials with exactly these properties. This allows us to numerically test our predictions. Moreover, this provides a playground for quasi-single field models of inflation, because higher order couplings can be tuned as well. As far as we know, no exact models of QSF are known.

- Chapter 3: we study Orbital Inflation (see Chapter 2) in the limit that the entropy mass is zero. We dub this 'ultra-light Orbital Inflation' because these models realize the shift symmetry described in [138]. If the radius of curvature of the inflationary trajectory is sufficiently small, the amplitude of isocurvature perturbations and primordial non-Gaussianities are highly suppressed. These models mimic the predictions of single-field inflation, because only one degree of freedom is responsible for the observed perturbations. Inflation proceeds along an 'angular' isometry direction in field space at arbitrary radius and is a special case of Orbital Inflation discussed in Chapter 2. We prove neutral stability of a class of exact attractor solutions.

  The results in this chapter are based on joint work with Ana Achúcarro, Edmund Copeland, Oksana Iargyina, Gonzalo Palma and Dong-Gang Wang.

- Chapter 4: we investigate two-field cosmological α-attractors, which are characterized by a hyperbolic field metric. The important property of the single field realization of α-attractors is that, in the limit of small $\alpha < \mathcal{O}(10)$, their predictions converge to $n_s \simeq 1 - \frac{2}{N}$, $r \simeq \frac{4}{N^2}$. In the two-field case, we find that the inflationary predictions show universal behavior too, insensitive to significant modifications of the potential. In particular, when both fields are light, the multi-field effects conspire in such a way that the predictions remain unchanged with respect to the single field scenario. We emphasize the key role played by the hyperbolic field space. We also list the constraints on the potential to ensure the

validity of our results.

This chapter is based on [139]:
Universality of multi-field α-attractors, A. Achúcarro, R. Kallosh, A. Linde, D-G. Wang and Y. Welling, JCAP **1804** (2018) 07, 028, (arXiv:1711.09478 [hep-th]).

- Chapter 5: we illustrate the impact of heavy fields on the inflationary observables by a simple two-field embedding of a few large-field models of inflation. In our set-up the inflaton corresponds to the phase of a complex field with mildly broken $U(1)$ symmetry. This type of embedding affects the background evolution and modifies the effective sound speed of the curvature perturbation. The overall effect is that the tensor-to-scalar ratio is reduced, which improves the viability of the inflationary models under consideration.

  The results in this chapter are based on [140]:
  On the viability of $m^2\phi^2$ and natural inflation, A. Achúcarro, V. Atal and Y. Welling, JCAP **1507** (2015) 07, 008, (arXiv:1503.07486 [astro-ph.CO]).

Large scale structure

In Part II of this thesis we study the detectability of non-Gaussianities in near future large scale structure experiments, using the bispectrum as observable. In § 1.4 we describe how the primordial perturbations from inflation evolve into the large scale structures we see around us today. To extract information about the early universe we have to understand the relation between the distribution of galaxies and the primordial power spectrum and bispectrum. One of the ingredients is to understand the clustering of dark matter. On the largest scales this is well captured by linear perturbation theory. We review the main idea of the 'Effective Theory of Large Scale Structure' (EFT of LSS), a theoretical method that extends the perturbative description to quasi non-linear scales.

- Chapter 6: we perform a simple statistical analysis to understand whether the EFT of LSS can help us to improve the constraints on primordial non-Gaussianities in upcoming surveys such as Euclid. As a first step we focus exclusively on the matter bispectrum. Already in this simplified set-up we find that it is unlikely to reach the theoretical benchmarks quoted between Eq. 1.42 and Eq. 1.43. On the other hand, the EFT reduces the size of the error bars by a factor of 3 compared to standard perturbation theory (SPT) in this set-up. We put special emphasis on

the modeling of theoretical uncertainties.

The results in this chapter are based on [141]:
Lifting Primordial Non- Gaussianity Above the Noise, Y. Welling, D. van der Woude, and E. Pajer, JCAP **1608** (2016) 08, 044, (arXiv:1605.06426 [astro-ph.CO]).

1.4 Large scale structure as a probe of inflation

After inflation produced the tiny initial density inhomogeneities, they slowly evolved into the structures we see around us today. The current picture of structure formation is based on work by Zeldovich, Peebles and collaborators [33, 142–144]. It is believed that gravitational instability drives cold dark matter to evolve into large scale filaments. In this network, structures form through hierarchical clustering of small objects, such as galaxies. With our telescopes we observe light coming from these galaxies, and they trace the underlying network of dark matter. This allows us to connect the observed galaxy distribution with the dark matter distribution, which in its turn probes the initial conditions set by inflation.

However, extracting information about the primordial universe is challenging. There are several complex steps that have to be understood in order to make connection with the observational data. The first step we have to understand is the non-linear gravitational evolution of dark matter overdensities. Second, galaxies[10] only form in the densest regions, and are therefore biased tracers of the dark matter distribution. Finally, there are observational complexities, such as redshift space distortions and projection effects.

Fortunately, on sufficiently large scales, gravitational evolution, biasing and redshift space distortions are controllable by perturbative methods [145–147]. Since our aim is to learn something about inflation[11], we are mainly interested in these large scales, where the imprint of initial conditions has not been much distorted yet. This calls for a theoretical description that captures both initial conditions and gravitational evolution by a finite number of parameters.

[10] Or any other tracer of dark matter.

[11] Of course, from the mildly non-linear scales there is more to learn about cosmology than just inflation. For instance, the shape and the location of the Baryon Acoustic Oscillations (BAO) in the range $k \sim 0.05 - 0.25h\text{Mpc}^{-1}$ provides a powerful probe of the properties of dark energy [148].

In this thesis we focus exclusively on the gravitational evolution of dark matter.

Depending on how far we can push the analytical description, large scale structure (LSS) surveys have the potential to become competitive with the CMB. The main advantage is that LSS surveys are three dimensional, and therefore they contain in principle much more information. The number of independent measurements we can extract from the CMB scales roughly as $N_{\rm CMB} \sim (k_{\rm max}/k_{\rm min})^2 \sim 10^7$, whereas in LSS[12] it scales like $N_{\rm LSS} \sim (k_{\rm max}/k_{\rm min})^3$. This means that if we can push $k_{\rm min}$ closer to the non-linear scale $k_{\rm NL} \sim 0.2h{\rm Mpc}^{-1}$ (see § 1.4.1) and map the largest volume $k_{\rm min} \sim \frac{H}{c} \sim 10^{-4}h{\rm Mpc}^{-1}$, we might even approach a factor $\mathcal{O}(10^2)$ more datapoints with respect to the CMB.

To describe the evolution of dark matter on mildly non-linear scales, we employ Eulerian perturbation theory. In this framework, dark matter is modelled as a self-gravitating effective fluid on large scales (see § 1.4.2). In its first formulation in the nineties, dark matter was assumed to take the form of a pressureless perfect fluid. This resulted in Standard Perturbation Theory (SPT), for a comprehensive review see [149]. With the increasing precision of (future) LSS surveys [68, 130, 150–152], several improvements on SPT were proposed in the following decades, see e.g. [153–165]. In particular, it was realized [159, 166–168] that SPT is limited by the assumption that dark matter can described in terms of density and velocity perturbations only. For instance, SPT assumes a vanishing velocity dispersion. However, the velocity dispersion was shown to give percent level corrections to the predictions of SPT [166]. Therefore, this should be incorporated in the analytical description as well. More generally, we should take into account the backreaction of the short scale physics on the dynamics of the dark matter fluid.

This has led to the development of several new perturbation techniques, among which the so-called Effective Theory of Large Scale Structures (EFT of LSS) [159, 162]. The backreaction of short scale physics is captured by an effective viscous shear tensor in the fluid equations. By expanding the stress tensor in terms of the long wavelength density and velocity perturbations, the fluid equations become an effective description of dark matter, valid on large scales. The small and large scales become correlated during their joint gravitational evolution, and might also be correlated initially in the presence of primordial non-Gaussianities.

[12] This is a naive estimate of the number of independent measurements, neglecting shot-noise and cross-correlations.

In this section we review some elements of perturbation theory relevant for Chapter 6. In § 1.4.1 we show the behavior of the transfer function, which captures the linear evolution of the matter density perturbation from the primordial to the late universe. This allows us to estimate the non-linear scale at which the density perturbations become order unity. In § 1.4.2 we recap how to describe dark matter as a fluid on scales larger than the non-linear scale. In particular, we pay special attention to the smoothing procedure and the appearance of an effective stress tensor. After expanding the stress tensor in terms of the long wavelength fields, we can solve the fluid equations perturbatively. In § 1.4.3 we show how to compute a non-linear correction to the power spectrum. Finally, in § 1.4.4 we discuss shortly the bispectrum, which is the topic of Chapter 6.

1.4.1 Transfer Function

During most of the history of the universe the matter density perturbations were tiny $\delta_m \ll 1$. Only during the epoch of matter domination they started to grow substantially and form the non-linear structures. The linear evolution from the initial conditions from inflation to the late universe (well after matter-radiation equality) can be captured by the *transfer function*

$$\delta_{m,\mathbf{k}}(a) = \frac{2}{5\Omega_m}\frac{k^2}{a^2H^2}T_\delta(k)\mathcal{R}_\mathbf{k} \ . \tag{1.49}$$

It is conventional to factor out some terms, such that the transfer function asympotes to unity on large scales and only depends on k otherwise. Let's recap how the transfer function scales with k. We follow the set of lectures by Baumann [70], where everything is more rigorously derived[13]. First of all, the Poisson equation relates the evolution of the perturbed energy density to the gravitational potential as $\nabla^2\Phi = a^2\delta\rho/M_p^2$. Assuming we are in the epoch of matter domination or later, we can replace $\delta\rho = \bar{\rho}_m\delta_m$, because the contribution from radiation is negligible and dark energy does not cluster.

[13] In short, in § 1.4.1 we work in Newtonian gauge in conformal time $ad\tau = dt$

$$ds^2 = a^2(\tau)\left[(1+2\Psi)d\tau^2 - (1-2\Phi)\delta_{ij}dx^i dx^j\right], \tag{1.50}$$

where we assume the absence of anisotropic stress, which implies $\Psi = \Phi$. The tensor and vector modes are neglected. Here Φ corresponds to the Newtonian potential in the weak field limit. When we map the inflationary predictions to the late universe, the variables we work with have to be understood as gauge invariant variables. The gravitational potentials are indentified with the Bardeen variables [169] and the curvature perturbation and density perturbation are the *comoving* curvature perturbation [86] and density perturbation Δ_m. On sub-Hubble scales $\Delta_m \approx \delta_m$.

Going to Fourier space and using the Friedmann equation Eq. 1.8 we rewrite the Poisson equation as

$$\delta_{m,\mathbf{k}} = -\frac{2k^2}{3a^2\Omega_m H^2}\Phi_{\mathbf{k}} \ . \tag{1.51}$$

The evolution of the gravitational potential directly translates to that of δ_m. The linear dynamics of the gravitational potential turns out to be quite simple. First of all, on super Hubble scales the gravitational potential Φ is related to the curvature perturbation as follows

$$\mathcal{R} = -\frac{5+3w}{3+3w}\Phi, \tag{1.52}$$

where w is the equation of state of the background. Assuming adiabatic[14] initial conditions, this implies that the gravitational potential is conserved on super Hubble scales, as long as the equation of state is constant. In the transition from radiation to matter Φ however drops by a factor of 9/10, because $\mathcal{R}$ remains constant. The evolution of the gravitational potential on all scales is captured by the Einstein equations. It can be shown that the gravitational potential is constant throughout the matter era. If perturbations become sub-Hubble at that time we therefore have the simple relation[15] $\Phi_{\mathbf{k}} = -\frac{3}{5}\mathcal{R}_{\mathbf{k}}$ which yields

$$\delta_{m,\mathbf{k}} = \frac{2}{5\Omega_m}\frac{k^2}{a^2H^2}\mathcal{R}_{\mathbf{k}} \ . \tag{1.53}$$

On the other hand, if the gravitational potential enters the horizon (at $k\tau = -1$) during the radiation era it decays as τ^{-2} until matter-radiation equality. Therefore, in this case the gravitational potential receives an additional suppression $\Phi_{\mathbf{k}} \sim (k_{\rm eq}/k)^2$. This results in the following approximate asymptotic scalings [114]

$$T_\delta(k) = 1 \qquad \text{for } k \ll k_{\rm eq}, \tag{1.54a}$$

$$T_\delta(k) \approx 12\left(\frac{k_{\rm eq}}{k}\right)^2 \ln\left(\frac{k}{8k_{eq}}\right) \qquad \text{for } k \gg k_{\rm eq} \ . \tag{1.54b}$$

Here the logarithmic correction reflects the logarithmic growth of matter perturbations during radiation domination. Improved theoretical fitting functions are given in [170, 171]. Exact transfer functions can be computed numerically with CMBFAST [172] or CAMB [173]. If we set initial conditions well in the

[14] See the discussion around Eq. 1.46.

[15] This explains the funny normalization of f_{NL} in Eq. 1.40.

epoch of matter domination, the linear dimensionless matter power spectrum is therefore given by

$$\Delta_\delta^2(k,\tau) = \frac{4}{25\Omega_m^2}\frac{k^4}{a^4H^4}T_\delta^2(k)\Delta_{\mathcal{R}}^2(k) \tag{1.55}$$

Its exact behavior, computed using CAMB [173], is shown in Figure 1.4. The scaling of Δ_δ^2 agrees qualitatively with that of Eq. 1.54b. Around the scale of matter-radiation equality the power spectrum bends over from power law growth $(k/k_{eq})^4$ to logarithmic growth $\ln(k/k_{eq})$.

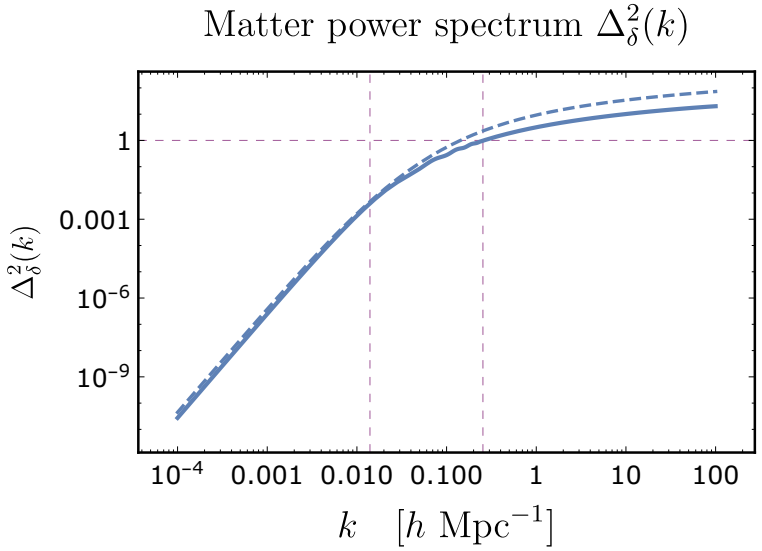

Figuur 1.4: The linear dimensionless matter power spectrum today $\Delta_\delta^2(k,\tau_0)$ (solid line) generated with the online tool of CAMB [173]: `http://lambda.gsfc.nasa.gov/toolbox/tb_camb_form.cfm`. We used $\Omega_\Lambda^0 = 0.728$, $\Omega_b^0 = 0.046$, $\Omega_{dm}^0 = 0.226$, $\Omega_r^0 = 8.4\cdot10^{-5}$, $n_s = 0.967$, $h = 0.704$ and $\sigma_8 = 0.81$. We indicate the scale of matter-radiation equality $k_{\mathrm{eq}} \approx 0.073 h\Omega_m^0\ h\mathrm{Mpc}^{-1}$ [114] and the non-linear scale $k_{\mathrm{NL}} \approx 0.25\ h\mathrm{Mpc}^{-1}$, at which $\Delta_\delta^2(k_{\mathrm{NL}},\tau_0) = 1$. Moreover, we compare with the result we get by using a transfer function that has the asymptotic limits quoted in Eq. 1.54b (dashed line). More precisely, we used $T(x \equiv \frac{k}{8k_{eq}}) = \frac{\ln(1+x)}{x}\left(1+\frac{2}{3}x\right)^{-1}$, which we inserted into Eq. 1.55.

Non-linear scale

Note from Eq. 1.51, that, even though the amplitude of the gravitational potential is always $\Delta^2_\Phi(k) \sim 10^{-9} T^2_\delta(k)$, the amplitude of density fluctuations is much larger and grows with a^2 during matter domination, where $H^2 \sim \rho_m \sim a^{-3}$. Today the linear matter power spectrum exceeds unity at the *non-linear scale* $k_{\rm NL} \approx 0.25\ h{\rm Mpc}^{-1}$. This signals the breakdown of the linear approximation, or more precisely the breakdown of perturbation theory in the density contrast δ_m. To make sensible theoretical predictions within perturbation theory, we need to consider sufficiently large scales compared to the non-linear scale. We will next see how dark matter can be modeled as an effective fluid on these scales.

1.4.2 The Dark Matter Fluid

We assume that dark matter consists of a collection of non-relativistic particles of mass m, which interact only gravitationally. They can be described by the collisionless Boltzmann equation, or Vlasov equation [174]

$$\frac{Df}{D\tau} \equiv \frac{\partial f}{\partial \tau} + \frac{\mathbf{p}}{am} \cdot \nabla f + \partial_\tau \mathbf{p} \cdot \frac{\partial f}{\partial \mathbf{p}} = 0 \ . \tag{1.56}$$

Here $f(\tau, \mathbf{x}, \mathbf{p})$ is the particle number density in phase space, with $\mathbf{p} \equiv am\mathbf{v}$ the conjugate momentum to the comoving spatial coordinate $\mathbf{x}$ of the particle. Moreover, $\mathbf{v} = \partial_\tau \mathbf{x}$ denotes its peculiar velocity. Notice that the conjugate momentum can be related to the spatial part of the four momentum as $p^i = \delta^{ij} P_j$. We denote the partial derivative with respect to x^i as ∇_i and raise its index with δ^{ij}. This notation is commonly used in the literature. We limit ourselves to sub-Hubble scales, such that we can use the Newtonian limit of the geodesic equation $\partial_\tau \mathbf{p} = -am\nabla\Phi$ and the Poisson's equation $\nabla^2\Phi = a^2\delta\rho/M_p$ (see [174, 175]).

The position space equations can be obtained by taking successive moments of the Vlasov equation and replacing

$$\frac{1}{a^3}\int d^3\mathbf{p}\ m f(\tau, \mathbf{x}, \mathbf{p}) = \rho(\tau, \mathbf{x}), \tag{1.57a}$$

$$\frac{1}{a^3}\int d^3\mathbf{p}\ \frac{p^i}{a} f(\tau, \mathbf{x}, \mathbf{p}) = \rho v^i(\tau, \mathbf{x}) \equiv \pi^i(\tau, \mathbf{x}), \tag{1.57b}$$

$$\frac{1}{a^3}\int d^3\mathbf{p}\ \frac{p^i p^j}{a^2 m} f(\tau, \mathbf{x}, \mathbf{p}) = \rho v^i v^j(\tau, \mathbf{x}) + \rho\sigma^{ij}(\tau, \mathbf{x}), \tag{1.57c}$$

etc ....

Here we implicitly assumed some spatial smoothing of the phase space distribution function [16] in order to define the mass density ρ and mean peculiar momentum density π^i. This induces velocity dispersion σ^{ij} because there are multiple individual particle velocities in a given spatial patch. Moreover, there could already be a microscopic velocity dispersion if particle trajectories cross [168]. It has been estimated numerically [166] and theoretically [167] that velocity dispersion induces a percent level correction to large scale matter power spectrum at $k \sim 0.1h\text{Mpc}^{-1}$. This means that we have to take it into account in our theoretical description.

Taking moments of the Vlasov equation generates an infinite set of evolution equations (the *Boltzmann hierarchy*) which couple the moments of the distribution function to each other. To arrive at the fluid description, we neglect the higher moments contained in the dots of Eq. 1.57, such that the full Boltzmann hierarchy is reduced to the Euler equations. This is possible as long as we pick a smoothing scale larger than the distance that dark matter particles have travelled $1/k \gg v_p/aH$ [159, 168, 176]. Here v_p is the typical size of the peculiar velocity of the dark matter particles, and $\frac{\mathcal{O}(1)}{aH}$ represents the particle horizon since reheating. Using linear theory (see § 1.4.3) one can estimate $\Delta_v^2 \sim \frac{a^2H^2}{k^2}\Delta_\delta^2$, and therefore, if we only consider scales larger than the non-linear scale, this suggests that the fluid description is applicable, taking $v_p \lesssim \sqrt{\Delta_v^2(k_{NL})} \sim aH/k_{NL}$. The intuitive interpretation of [159] is that dark matter has an effective mean free path of the order of the non-linear scale, because of the finite horizon induced by gravity. Higher moments are suppressed, because they did not have time to develop.

[16] The microscopic phase space distribution for a collection of particles is given by the Klimontovich density

$$f(\tau, \mathbf{x}, \mathbf{p}) = \sum_n \delta^{(3)}(\mathbf{p} - \mathbf{p}_{(n)})\delta^{(3)}(\mathbf{x} - \mathbf{x}_{(n)}) \,. \tag{1.58}$$

To get the coarse-grained stress tensor in some comoving ball ΔV around $\mathbf{x}$ we are effectively smoothing f. For instance, with a spherical top-hat window function

$$\langle T_{\mu\nu}\rangle(\mathbf{x}) = \int_{\Delta V} \frac{d^3\mathbf{x}'}{\Delta V} \int \frac{\Pi_j dP_j}{\sqrt{-g}} \frac{P_\mu P_\nu}{P^0} f(\mathbf{x}', \mathbf{p}, \tau) = \frac{1}{a^4 \Delta V} \sum_n \left. \frac{P_\mu^{(n)} P_\nu^{(n)}}{P^0_{(n)}} \right|_{\mathbf{x}^{(n)} \in \Delta V} \,. \tag{1.59}$$

Euler Equations

Truncating the Boltzmann hierarchy at the second moment allows us to describe the dynamics of dark matter on sufficiently large scales by the continuity equation and Euler equation

$$\partial_\tau \rho + 3aH\rho + \nabla_i(\rho v^i) = 0, \tag{1.60a}$$

$$\rho\partial_\tau v^i + aH\rho v^i + \rho v^j \nabla_j v^i + \rho\nabla^i\Phi = -\nabla_j \tau_\Lambda^{ij} \ . \tag{1.60b}$$

The index Λ on the stress tensor τ_Λ^{ij} emphasizes that we have smoothed the Vlasov equation on a scale $\Lambda \ll k_{NL}$. The resulting long wavelength fields ρ, v and Φ variables should also carry an index ℓ (for *long*), but we dropped it to avoid cluttering of notation. Importantly, smoothing the Vlasov equation creates an *effective stress tensor* in the Euler equation. For instance, the smoothing of the part that is responsible for the term $\sim \rho vv$ induces velocity dispersion as we saw above. We will see below that a similar story applies to the term $\sim \rho\Phi$. The other terms in the Euler equations are linear in ρ or π^i. Therefore, we end up with an effective stress tensor τ_Λ^{ij} that captures the velocity dispersion and the gravitationally induced stress, and also contains contributions from the higher moments that we have neglected.

Smoothing the Vlasov Equation

We smooth the Vlasov equation because it allows us to truncate the Boltzmann hierarchy. To understand the appearance of the effective stress tensor and its structure, we follow [159, 162] and see what happens if we smooth with a Gaussian window function

$$W_\Lambda(\mathbf{x}) = \left(\frac{\Lambda}{\sqrt{2\pi}}\right)^3 e^{-\frac{1}{2}\Lambda^2 x^2} \text{ or in Fourier space } \quad W_\Lambda(\mathbf{k}) = e^{-\frac{1}{2}\frac{k^2}{\Lambda^2}} \ . \tag{1.61}$$

This provides a smooth cut-off $k \sim \Lambda$ in Fourier space. Smoothed quantities are defined as

$$O_\Lambda(\mathbf{x},\tau) \equiv \int d^3\mathbf{x}' W_\Lambda(\mathbf{x}-\mathbf{x}')O(\mathbf{x}',\tau) \quad \text{or} \quad O_\Lambda(\mathbf{k},\tau) = W_\Lambda(\mathbf{k})O(\mathbf{k},\tau) \ . \tag{1.62}$$

The goal is to express the Euler equations in terms of long wavelength fields ρ_ℓ, v_ℓ and Φ_ℓ only, such that we can perturbatively solve the fluid equations.

Notice that Eq. 1.57 naturally defines $\rho_\ell = \rho_\Lambda$, $\rho_\ell v_\ell = \pi_\Lambda$ and $\rho_\ell \sigma_\ell^{ij} = (\rho\sigma^{ij})_\Lambda$. It is what we get if we convolve the moments of the phase space distribution with the window function. This means that the long wavelength

peculiar velocity is implicitly defined as $v_\ell \equiv \frac{\pi_\Lambda}{\rho_\Lambda}$. Furthermore, we define $\Phi_\ell = \Phi_\Lambda$. When smoothing the Vlasov equation we encounter the terms $(\rho\partial_i\Phi)_\Lambda$ and $(\rho v^i v^i)_\Lambda$ which are *not* the same as a products of the corresponding long wavelength fields. For instance, smoothing a bilinear quantity fg yields [159]

$$(fg)_\Lambda = f_\ell g_\ell + (f_s g_s)_\Lambda + \frac{1}{\Lambda^2}\nabla f_\ell \cdot \nabla g_\ell + \dots , \tag{1.63}$$

where the dots represent higher derivative terms. The short wavelength fields are defined as $f_s \equiv f - f_\ell$. The same can be computed for trilinears. It has been shown that with this smoothing procedure the stress tensor receives contributions of the form [159, 168, 177]

$$\tau^{ij}_\Lambda \supset -\left(\rho v^i_s v^j_s + \tfrac{M_p^2}{a^2}\left(\delta^{ij}\nabla_k\Phi_s\nabla^k\Phi_s - 2\nabla^i\Phi_s\nabla^j\Phi_s\right) + \rho\sigma^{ij}_s\right)_\Lambda + \dots \ . \tag{1.64}$$

The dots represent the derivative terms suppressed by $(k/\Lambda)^2$. These derivative terms are very small, because they contain two or more powers of the long wavelength fields, where at least one of them is v_ℓ or Φ_ℓ.

Effective Theory of Large Scale Structure

From Eq. 1.64 we see that the effective stress-tensor captures the backreaction of the short scale physics on the dynamics of dark matter on the largest scales. By construction, we cannot evaluate Eq. 1.64 within perturbation theory. Therefore, the next step is to parameterize our ignorance of the small scales by expanding the stress tensor in terms of the long wavelength fields in the most generic way allowed by symmetries. This is where the so-called Effective Theory of Large Scale Structure (EFT of LSS) [159, 162] comes in.

What kind of contributions do we expect from the microscopic theory? Let's zoom in on a random small comoving box of particles of size $\sim 1/\Lambda^3$ which evolves in a background of a long wavelength gravitational potential Φ_ℓ. The worldlines of the particles inside the box are affected by long wavelength tidal fields and this changes the distribution of velocities. They also experience a common acceleration by the gradient of the gravitational potential , but this is locally unobservable. Averaging over many of these boxes, given a realization of the long wavelength perturbations, this results in a shear tensor correlated with the tidal field [159]

$$\langle(\rho v^i_s v^j_s)_\Lambda|\Phi_\ell\rangle = \langle(\rho v^2_s)_\Lambda\rangle_0\left(c_1\delta_{ij} + c_2\frac{\nabla_i\nabla_j\Phi_\ell}{a^2H^2} + \dots\right) . \tag{1.65}$$

The first term contributes to the isotropic pressure, which is generated even in the absence of long wavelength perturbations. The second term is an example

of how the short scale physics feels the background of long modes in which they evolve, and how this is memorized in their backreaction.

More generally, one can write down all operators on the right hand side of the Euler equation that are allowed by the equivalence principle [159,162,178]. Local observables can only be affected by tidal forces $\nabla_i\nabla_j\Phi$ (or equivalently the shear $\nabla_i v_j$ [179]) and their spatial derivatives. To linear order in perturbations, up to higher derivative terms, this results in the Navier-Stokes equations with an average stress-tensor

$$\langle(\tau_{ij})_\Lambda|\delta_\ell,\ldots\rangle = p(\tau)\delta^{ij} + \rho\left[c_s^2(\Lambda,\tau)\delta_\ell\delta^{ij} - c_{bv}^2(\Lambda,\tau)\frac{\nabla_k v_\ell^k}{aH}\delta^{ij} - \frac{3}{2}c_{sv}^2(\Lambda,\tau)\frac{\nabla^{(i}v_\ell^{j)} - \frac{1}{3}\delta^{ij}\nabla_k v_\ell^k}{aH}\right] \tag{1.66}$$

Here the contraction $\nabla^2\Phi_\ell$ has been replaced by δ_ℓ, using the Poisson equation. It has been shown that the induced pressure $p(\tau) \sim 10^{-5}$ is tiny and has a negligible effect on the dynamics of the background [159], so we will ignore it further. For some observables a higher precision is required, and one needs to go beyond the linear expansion [180–182]. Moreover, when averaging over an ensemble of realizations of small domains, like we did in Eq. 1.65, we assumed that short scales only get correlated with the long modes through non-linear gravitational evolution. This is true as long as the initial short scale fluctuations are independent of the long wavelength perturbations. However, in the presence of primordial non-Gaussianities the short modes are correlated with the long wavelength perturbations through their dependence on the realization of the primordial potential [183]. The short scales memorize these initial conditions and this affects their backreaction on the evolution of the long modes.

The resulting EFT coefficients, such as $c_s^2(\Lambda,\tau)$, explicitly depend on the unphysical smoothing scale Λ. This is important, because if we compute observable quantities, such as the power spectrum, we will at the same time encounter loop integrals that are bounded by the scale Λ. For a well-defined perturbation theory, these dependencies on Λ should cancel. We will see that this is the case for the simplest contribution to the power spectrum in § 1.4.3. Internal consistency of the EFT of LSS has been demonstrated explicitly for the power spectrum up to two loop [178, 180, 184], for the one loop bispectrum [181–183] and eventually to all orders in perturbation theory in [185].

Scalings with $k/k_{\rm NL}$

Let's find out the relative importance of terms in the Euler equation by comparing their scaling with $k/k_{\rm NL}$. For simplicity we consider scales $k_H < k < k_{\rm eq}$ such that $\Phi \sim 10^{-5}$. On smaller scales we saw in § 1.4.1 that its amplitude is even more suppressed. First of all, at linear scales we have (using the results from § 1.4.1 and § 1.4.3

$$\Delta^2_\delta \sim \left(\frac{k}{aH}\right)^4 \Delta^2_\Phi \quad \text{and} \quad \Delta^2_v \sim \left(\frac{k}{aH}\right)^2 \Delta^2_\Phi \quad \text{with} \quad , \tag{1.67}$$

indicating that velocities and the gravitational potential remain small even when Δ^2_δ gets close to unity. This allows us to compare the various terms in the Euler equation, using that $\delta \sim (k/k_{\rm NL})^2$ and $\frac{\nabla\Phi}{aH} \sim v \sim \sqrt{\delta\Phi}$ [159, 162]

- The non-linear terms on the left-hand side of the Euler equation Eq. 1.60b scale like δ compared to the friction term

$$\frac{v\nabla v}{aHv} \sim \frac{\delta\nabla\Phi}{aHv} \sim \delta \tag{1.68}$$

- The linear terms in the stress tensor

$$c_s^2\frac{\nabla\delta}{aHv} \sim c_v^2\frac{\nabla\nabla v}{a^2H^2v} \sim c^2\frac{\delta}{\Phi}, \tag{1.69}$$

  where the coefficients are a measure of kinetic and gravitational stress induced by the short scales. For instance, in the example of Eq. 1.65, we would get $c^2 \sim \langle v_s^2\rangle$. At the non-linear scale we expect the velocity to approach $v^2 \sim \Phi$. The same applies to virialized scales, where the kinetic and gravitational energy are of the same order. Therefore, a rough estimate is $c^2 \sim \Phi \sim 10^{-5}$. This suggests that the leading terms in the stress tensor scale like δ as well.

- Higher order corrections to the stress tensor come with additional powers of derivatives $(k/k_{\rm NL})^2$ and long wavelength fields, so they are additionally suppressed.

1.4.3 Perturbation Theory

With all the ingredients at hand we can do perturbation theory in the long wavelength perturbations ρ_ℓ, $\mathbf{v}_\ell$ and Φ_ℓ. For that purpose it is convenient to define the long wavelength density contrast, velocity divergence and vorticity as

$$\delta_\ell \equiv \frac{\rho_\ell - \bar\rho}{\bar\rho}, \quad \theta_\ell \equiv \nabla\cdot\mathbf{v}_\ell, \quad \text{and} \quad \mathbf{w}_\ell \equiv \nabla\times\mathbf{v}_\ell, \tag{1.70}$$

respectively. For notational convenience we drop the index ℓ from now on. Using Eq. 1.66, the leading order source term of the Euler equation Eq. 1.60b is given by

$$\frac{1}{\rho}\nabla_j \tau_\Lambda^{ij} \approx c_s^2 \nabla^i \delta - \frac{4c_{bv}^2 + c_{sv}^2}{4aH}\nabla^i\theta - \frac{3c_{sv}^2}{4aH}\nabla^2 v^i + J^i, \tag{1.71}$$

with $J^i = \frac{1}{\bar{\rho}}\nabla_j \Delta\tau^{ij}$ a stochastic term to account for the fact that the stress tensor is not precisely equal to its ensemble average over the short scales, i.e. $(\tau^{ij})_\Lambda = \langle (\tau^{ij})_\Lambda | \delta_\ell, \ldots \rangle + \Delta\tau^{ij}$. After subtracting the background evolution of $\bar{\rho}$ using Eq. 1.2b we obtain equations for the density contrast, velocity divergence and vorticity. First of all, the equation of motion for vorticity reads [177]

$$\left(\partial_\tau + aH - \frac{3c_{sv}^2}{4aH}\nabla^2\right)\mathbf{w} = \nabla \times (\mathbf{v} \times \mathbf{w} - \mathbf{J}) \ . \tag{1.72}$$

In the absence of the terms on the right hand side, vorticity decays [149] (assuming $c_{sv}^2 > 0$). If it is not present initially it may be generated by the stochastic term, or by the higher order terms in the effective stress tensor [177]. However, numerical studies [166] find a negligible amount of vorticity on the larger scales, which gives less than a 0.01% correction to the matter power spectrum at $k \sim 0.1h\mathrm{Mpc}^{-1}$, so we neglect it.

The Euler equations Eq. 1.60 simplify considerably and in Fourier space they read

$$\partial_\tau \delta + \theta = S_\alpha, \tag{1.73a}$$

$$(\partial_\tau + aH)\theta + \frac{3}{2}\Omega_m a^2 H^2 \delta = S_\beta + c_s^2 k^2 \delta - c_v^2 \frac{k^2\theta}{aH} - J \ , \tag{1.73b}$$

where the two viscocity coefficients are combined into one $c_v^2 = c_{sv}^2 + c_{bv}^2$ and the stochastic term is contracted to the scalar $J = \frac{1}{\bar{\rho}}\nabla_i \nabla_j \Delta\tau^{ij}$. The SPT source terms are given by [149]

$$S_\alpha(\mathbf{k},\tau) = -\int_{\mathbf{p}} \frac{\mathbf{p}\cdot\mathbf{k}}{p^2}\theta(\mathbf{p},\tau)\delta(\mathbf{k}-\mathbf{p},\tau), \tag{1.74a}$$

$$S_\beta(\mathbf{k},\tau) = -\int_{\mathbf{p}} \frac{k^2\mathbf{p}\cdot(\mathbf{k}-\mathbf{p})}{p^2(\mathbf{k}-\mathbf{p})^2}\theta(\mathbf{p},\tau)\theta(\mathbf{k}-\mathbf{p},\tau). \tag{1.74b}$$

The equations can be solved perturbatively using Green's functions, and the solution can be written in terms of a power series of the initial density contrast $\delta_1(\mathbf{k}) = \delta(\mathbf{k},\tau_{\mathrm{in}})$

$$\delta(\mathbf{k},\tau) = \sum_n \delta^{(n)}(\mathbf{k},\tau), \qquad \theta(\mathbf{k},\tau) = \sum_n \theta^{(n)}(\mathbf{k},\tau) \ . \tag{1.75}$$

The n-th order solution receives SPT, viscosity and noise contributions (and mixing terms, but they do not appear at the order we consider now)

$$\delta^{(n)}(\mathbf{k},\tau) = \delta^{(n)}_{\rm SPT}(\mathbf{k},\tau) + \delta^{(n)}_{c}(\mathbf{k},\tau) + \delta^{(n)}_{J}(\mathbf{k},\tau) \tag{1.76}$$

The linear solutions are obtained by setting the right-hand side of Eq. 1.73 to zero, i.e. $\delta^{(1)}(\mathbf{k},\tau) = \delta^{(1)}_{\rm SPT}(\mathbf{k},\tau)$. The contributions from the stress-tensor are treated as a next-to-leading-order correction, since they are derivatively suppressed.

SPT Solution

The SPT solutions are obtained by putting the effective stress tensor to zero. To a remarkable good approximation they are of the separable form [149]

$$\delta^{(n)}_{\rm SPT}(\mathbf{k},\tau) \approx D_1^n(\tau)\delta_n(\mathbf{k}), \tag{1.77a}$$

$$\theta^{(n)}_{\rm SPT}(\mathbf{k},\tau) \approx -aHf(\tau)D_1^n(\tau)\theta_n(\mathbf{k})\ . \tag{1.77b}$$

Here $D_1(\tau)$ is the linear growth factor and $f(\tau)$ its logarithmic derivative with respect to the scale factor. In a universe filled with matter and dark energy only ($\Omega_m + \Omega_\Lambda = 1$) the growing mode solutions are given by [186–188]

$$D_1(a) = \frac{5\Omega_m^0}{2}H_0^2H(a)\int_{a_{\rm in}}^{a}\frac{d\tilde{a}}{\tilde{a}^3H^3(\tilde{a})} \quad \text{and} \quad f(a) \equiv \frac{d\ln D_1(a)}{d\ln a} \approx \Omega_m^{5/9}(a)\ . \tag{1.78}$$

Furthermore, the initial conditions δ_n and θ_n are convolutions of multiple δ_1's with the SPT kernel functions F_n and G_n (please see [149] for their explicit form)

$$\delta_n(\mathbf{k}) = \int_{\mathbf{p}_1}\cdots\int_{\mathbf{p}_n}(2\pi)^3\delta_D^{(3)}(\mathbf{k}-\mathbf{p}_{1\ldots n})F_n(\mathbf{p}_1,\cdots\mathbf{p}_n)\delta_1(\mathbf{p}_1)\cdots\delta_1(\mathbf{p}_n), \tag{1.79a}$$

$$\theta_n(\mathbf{k}) = \int_{\mathbf{p}_1}\cdots\int_{\mathbf{p}_n}(2\pi)^3\delta_D^{(3)}(\mathbf{k}-\mathbf{p}_{1\ldots n})G_n(\mathbf{p}_1,\cdots\mathbf{p}_n)\delta_1(\mathbf{p}_1)\cdots\delta_1(\mathbf{p}_n)\ . \tag{1.79b}$$

Remember that we are integrating over the long wavelength fields only, therefore each $\delta_1(p)$ implicitly carries a factor $W_\Lambda(p)$.

Notice that we can express the linear solution for the velocity field in terms of the gravitational potential. First, we saw in Eq. 1.72 that the vorticity decays on linear scales. This means that the linearized Euler equation must give a solution of the form $v^i \sim \nabla^i\Phi$. More precisely, using the SPT results from above we find

$$v^i_{(1)} = \frac{2f(\tau)}{3aH\Omega_m}\nabla^i\Phi\ . \tag{1.80}$$

Therefore, at the linear order the tidal tensor and shear tensor are proportional to each other.

EFT Solution

To leading order the EFT contributions coming from the stress-tensor are given by

$$\delta_c^{(1)}(\mathbf{k},\tau) = -\xi(\tau)k^2\delta_{\rm SPT}^{(1)}(\mathbf{k},\tau), \tag{1.81a}$$

$$\delta_J^{(1)}(\mathbf{k},\tau) = N(\mathbf{k},\tau)\ . \tag{1.81b}$$

Here $\xi(\tau)$ is a time integral over the Green's function corresponding to the Euler equations Eq. 1.73 convolved with a combination of the viscocity parameters $c_s^2(\tau)$ and $c_v^2(\tau)$. The viscocity contribution correlates with the long wavelength density contrast, whereas the noise term is uncorrelated.

Power Spectrum

Using the ingredients above we can compute the contributions to the matter power spectrum

$$\Delta_\delta^2(k,\tau) = \frac{k^3}{2\pi^2}\langle\delta(\mathbf{k},\tau)\delta(-\mathbf{k},\tau)\rangle' = \Delta_{11}^2+\Delta_{13}^2+\Delta_{22}^2+\Delta_{1c}^2+\Delta_{JJ}^2+\ldots, \tag{1.82}$$

where $\Delta_{mn}^2(k,\tau) \equiv \frac{k^3}{2\pi^2}\left(\langle\delta_{\rm SPT}^{(m)}(\mathbf{k},\tau)\delta_{\rm SPT}^{(n)}(-\mathbf{k},\tau)\rangle' + \text{perm.}\right)$, and the other two contributions come from contractions of $\delta_{\rm SPT}^{(1)}$ with δ_c, and δ_J with itself, respectively. The dots represent higher order terms that we have neglected. Furthermore, in this example we have assumed Gaussian initial conditions, so after Wick contracting initial density contrasts (the δ_1's), terms such as Δ_{12}^2 will vanish.

Notice that all the terms on the right-hand side of Eq. 1.82 individually depend on the unphysical smoothing scale Λ, because they are constructed from the long wavelength density fields. The Λ dependence should cancel if we add all terms, otherwise the perturbative description makes no sense. Fortunately, this can be ensured. To see how this works, let's consider the 'renormalization' of the sum of Δ_{13}^2 and Δ_{1c}^2. The renormalization of $\Delta_{22}^2+\Delta_{JJ}^2$ proceeds in a similar way. The two individual contributions are given by

$$\Delta_{13}^2(k,\Lambda) = 6\Delta_{11}^2(k,\Lambda)\int_{\mathbf{q}} F_3(\mathbf{k},\mathbf{q},-\mathbf{q})P_{11}(q,\Lambda), \tag{1.83a}$$

$$\Delta_{1c}^2(k,\Lambda) = -\xi(\tau,\Lambda)k^2\Delta_{11}^2(k,\Lambda)\ . \tag{1.83b}$$

For notational convenience we suppressed the τ argument of the power spectra. It is understood that $\Delta_{11}^2(k,\Lambda) = D_1^2(\tau)W_\Lambda^2(k)\Delta_{\rm in}^2(k)$. The initial conditions are set well in the epoch of matter domination, such that the assumption $\Omega_m + \Omega_\Lambda = 1$ applies. Let's switch from Gaussian smoothing to imposing

a hard cut-off, where the window function is replaced by a heaviside step function that becomes zero at the scale Λ. This means we can split $\Delta^2_{13}(k,\Lambda)$ and $\Delta^2_{1c}(k,\Lambda)$ in a cut-off dependent and a cut-off independent part

$$\Delta^2_{13}(k,\Lambda) = 6\Delta^2_{11}(k)\left(\int^{\infty}_{\mathbf{q},0} F_3(\mathbf{k},\mathbf{q},-\mathbf{q})P_{11}(q) - \int^{\infty}_{\mathbf{q},\Lambda} F_3(\mathbf{k},\mathbf{q},-\mathbf{q})P_{11}(q)\right), \quad (1.84a)$$

$$\Delta^2_{1c}(k,\Lambda) = -(\xi_{\rm ph}(\tau)+\xi_{\infty}(\tau,\Lambda))k^2\Delta^2_{11}(k)\ . \quad (1.84b)$$

For large wavenumbers $q \gg k$ the SPT kernel F_3 scales like $F_3(\mathbf{k},\mathbf{q},-\mathbf{q}) \sim \frac{k^2}{q^2}$ [189]. This ensures that we can indeed cancel the cut-off dependence with the EFT coefficient

$$\xi_{\infty}(\tau,\Lambda) = -6k^{-2}\int^{\infty}_{\mathbf{q},\Lambda} F_3(\mathbf{k},\mathbf{q},-\mathbf{q})P_{11}(q), \quad (1.85)$$

as long as we pick $\Lambda^2 \gg k^2$. The final result is therefore independent of the cut-off scale and we are left with a physical coefficient $\xi_{\rm ph}(\tau)$, that has to be fitted to observational data or numerics

$$\Delta^2_{13}(k,\Lambda) + \Delta^2_{1c}(k,\Lambda) = \Delta^2_{11}(k)\left(\xi_{\rm ph}(\tau)k^2 + 6\int^{\infty}_{\mathbf{q},0} F_3(\mathbf{k},\mathbf{q},-\mathbf{q})P_{11}(q)\right) \quad (1.86)$$

Of course we do not necessarily need to integrate up to infinity. We could also integrate up to the non-linear scale $k_{\rm NL}$, for instance, and this automatically redefines what we mean by $\xi_{\rm ph}(\tau)$. However, from a computational perspective it does not matter what integration limit we choose, considering that the integral converges in our universe.

Finally, we should mention that the time dependence of the physical EFT coefficients is not known. This is not a problem necessarily, it just means that they have to be fitted at every redshift separately. On the other hand, this might be a bit too unrestrictive. In the limit of an Einstein-de-Sitter universe ($\Omega_m = 1$) with power law initial conditions $\Delta^2_{\delta,\rm in} \sim k^{n+3}$, the time dependence of the EFT coefficients is fixed by symmetry [184]. For instance, the time dependence of $\xi_{\rm ph}$ is given by $\xi_{\rm ph} \sim D_1(\tau)^{\frac{1-n}{n+3}}$. Therefore, one may also consider to make an ansatz for its time dependence $\xi_{\rm ph}(\tau) \sim D_1(\tau)^p$ for some value of p.

1.4.4 Bispectrum

In Chapter 6 we focus on the bispectrum as observable to constrain primordial non-Gaussianities. One can apply the same machinery as in § 1.4.3 to find all contributions to the bispectrum up to a given order. The gravitational induced bispectrum with Gaussian initial conditions has been computed up to one loop in [190] (SPT) and [181, 182] (EFT). The bispectrum coming from primordial non-Gaussianities has been computed to one-loop in [191] (SPT) and [183] (EFT). Schematically, the perturbative theoretical prediction for the bispectrum is given by

$$B^{\rm th} = B^{\rm G}_{\rm SPT} + B^{\rm G}_{\rm EFT} + f_{\rm NL}\left(B^{\rm NG}_{\rm SPT} + B^{\rm NG}_{\rm EFT}\right). \tag{1.87}$$

With the introduction of primordial non-Gaussianities we are doing a double expansion in f_{NL} and k/k_{NL}. Therefore, the relative importance of the various contributions to the bispectrum is harder to assess. Moreover, the bispectrum is a three dimensional function. The one-loop correction to the primordial signal might be more relevant in the squeezed configuration than, say, in the equilateral configuration.

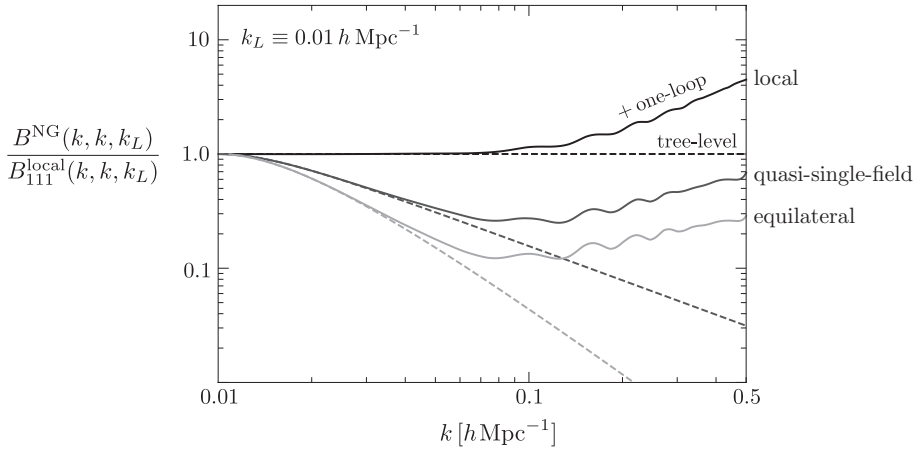

Figuur 1.5: Spectroscopy: comparison of the SPT one-loop corrected non-Gaussian bispectra (solid lines) for local, quasi-single-field and equilateral type of primordial non-Gaussianities. The dashed lines show the linearly evolved primordial bispectra. The gravitational distortions tend to decrease the difference between the various shapes. Moreover, the loop corrections kick in on relatively large scales. This Figure is taken from [183].

The gravitational distortion (one-loop SPT) of the primordial non-Gaussian signal is shown in Figure 1.5. We plot three different types of primordial non-Gaussianities, the local, equilateral and quasi-single-field templates defined in

Eq. 1.40, Eq. 1.41 and Eq. 1.42 (with $\nu = 1/2$), respectively. Figure 1.5 shows that the loop corrections become important already on relatively large scales. This was for us the main motivation to compute the EFT corrections to the one-loop bispectrum [183]. However, the gravitational distortions tend to decrease the difference between the three shapes. Therefore, we perform a simple statistical analysis in Chapter 6 to understand how much the EFT of LSS improves the modeling of the matter bispectrum, with the purpose of constraining primordial non-Gaussianities.